The Nesna Shear Zone, north-central Norway: an $^{40}Ar/^{39}Ar$ record of Early Devonian - Early Carboniferous ductile extension and unroofing

Elizabeth A. Eide, Per Terje Osmundsen, Gurli B. Meyer, Mark A. Kendrick & Fernando Corfu

Eide, E.A., Osmundsen, P.T., Meyer, G.B., Kendrick, M.A. & Corfu, F. The Nesna Shear Zone, north-central Norway: an $^{40}Ar/^{39}Ar$ record of Early Devonian – Early Carboniferous ductile extension and unroofing. *Norwegian Journal of Geology*, Vol. 82, pp. 317-339. Trondheim 2002. ISSN 029-196X.

In north-central Norway, $^{40}Ar/^{39}Ar$ ages from a profile through the Nesna Shear Zone (NSZ) and into the underlying Sjona window, a gneiss-cored culmination, document time of onset of ductile shearing and two episodes of unroofing for the crustal package. A progressive decrease in white mica and biotite ages from 397.8 ± 1.0 to 378.3 ± 0.9 Ma, downward through the tectonostratigraphy, conforms to an overall pattern of cooling and argon retention as the crustal section was progressively unroofed. The age differences between the NSZ and Sjona window micas allow us further to distinguish two kinematically distinct events. White mica and biotite ages within the NSZ fall between 397.8 ± 1.0 and 387.1 ± 0.8 Ma and correspond closely to time of genesis of the ductile, top-WSW stretching fabrics within the shear zone. Biotites within the Sjona window lack the same ductile fabric and instead record younger cooling largely between 384.3 ± 1.0 and 378.3 ± 0.9 Ma. Sjona window biotites passed through closure temperatures similar to those in the NSZ, but under conditions dominated by positive buoyancy of the Sjona gneisses, aided by shortening normal to the top-WSW stretching direction. Unroofing or 'doming' of the Sjona window was almost certainly promoted, and perhaps accelerated, by earlier, NSZ-related extension in the overlying nappe pile. Extension had waned by latest Mid Devonian time when the shear-zone system was overtaken by activity on younger, steeper, ductile-to-brittle extensional faults. K-feldspar ages from the Sjona window yield a pronounced Early Carboniferous signature (335-346 Ma) that we attribute to a second episode of rapid cooling and unroofing, after top-WSW ductile motion on the NSZ had ceased. We relate unroofing to motion on the steeper and younger faults that cut low-angle ductile shear zones like the NSZ. Early Carboniferous unroofing in north-central Norway would have been contemporaneous with widespread, Late Devonian-Early Carboniferous tectonic activity documented around the Caledonian perimeter. These mica and K-feldspar ages are the first published from north-central Norway and promote a picture of widespread, Early-Mid Devonian top-W to -SW ductile extension and latest Devonian-Early Carboniferous unroofing, operating at several tectonostratigraphic levels within the disintegrating Scandinavian Caledonide orogen.

Elizabeth A. Eide (elizabeth.eide@ngu.no), Per Terje Osmundsen, Gurli B. Meyer & Mark A. Kendrick, Geological Survey of Norway, Leiv Eirikssons vei 39, N-7491 Trondheim, Norway.
Fernando Corfu, Department of Geology, University of Oslo, Box 1047 Blindern, NO-0316 Oslo, Norway.

Introduction

In the Scandinavian Caledonides, long traditions of structural mapping and isotope geochronology have laid a foundation to address the complex changes in crustal temperature and composition, and deformation rates and styles intrinsic to the dynamic tectonic processes that formed the orogen. With a basis in well-defined tectonostratigraphy, U-Pb geochronology has been instrumental in defining the ages and origins of different igneous and metamorphic entities in this orogen until earliest Devonian time (e.g. Schärer 1980; Tucker et al. 1987, 1991; Dunning & Pedersen 1988; Corfu & Emmett 1992; Nordgulen et al. 1993). For Late Paleozoic and younger times, other isotopic techniques with lower nominal closure temperatures (e.g. $^{40}Ar/^{39}Ar$ and apatite fission-track) have contributed information about the emplacement and unroofing histories of different nappe units, the tectonic/denudational unroofing history of (par-) autochthonous basement, and timing of initiation and reactivation of regionally significant ductile and brittle faults (e.g. Dallmeyer et al. 1985; Dallmeyer 1990; Grønlie & Torsvik 1989; Grønlie et al. 1990; Chauvet & Dallmeyer 1992; Boundy et al. 1996; Fossen & Dunlap 1998; Dunlap & Fossen 1998; Eide et al. 1997; Hendriks et al. 2002; Redfield et al. in press).

Recently, high-precision $^{40}Ar/^{39}Ar$ geochronology combined with kinematic analysis has been applied in the Scandinavian Caledonides to address very specific questions about the timing and mechanisms of syn- and post-collisional tectonics. These studies have included analysis of: 1) timing and kinematics of contractional versus extensional activity in foreland and hinterland in southern and western Norway (Fossen & Dall-

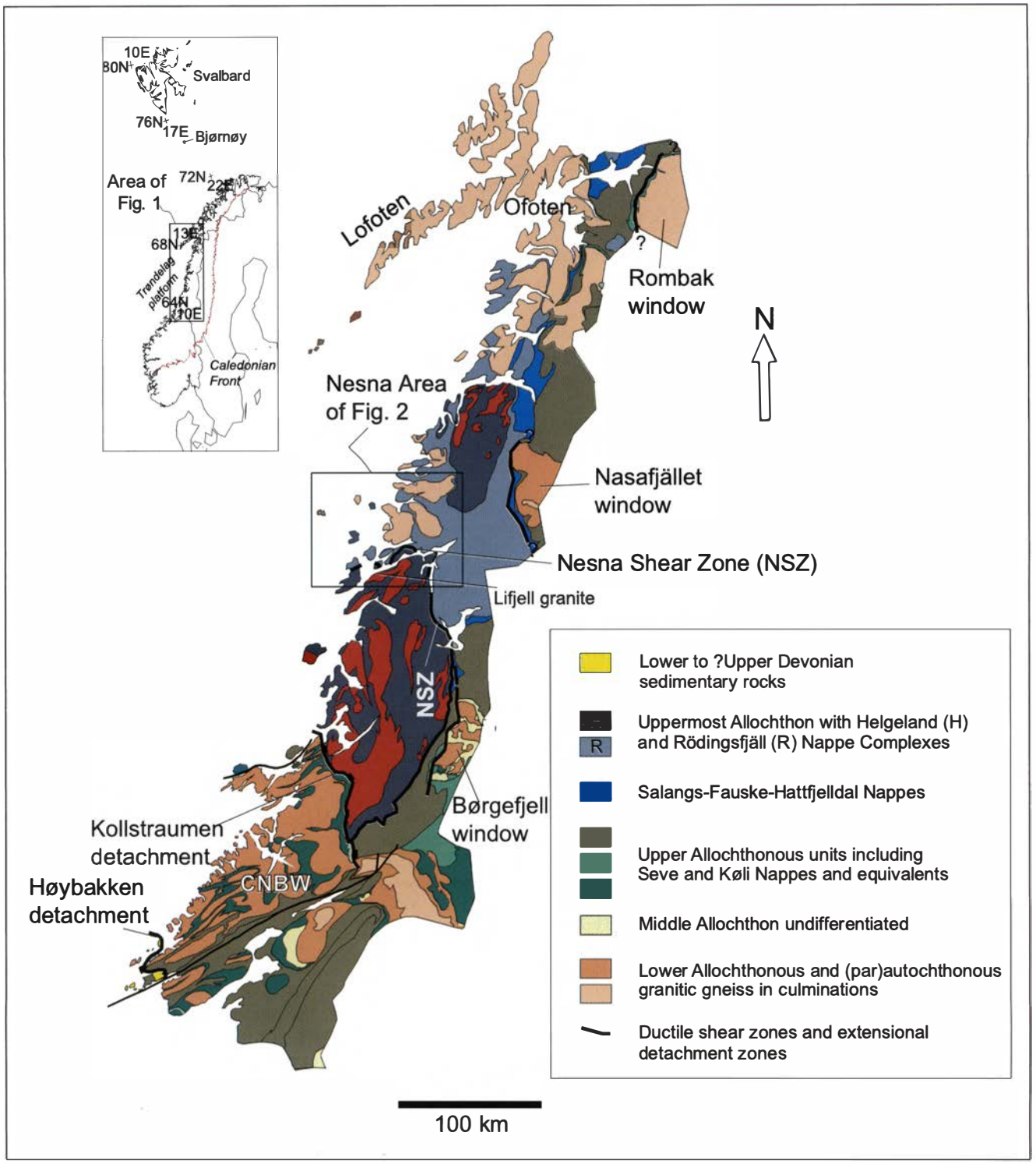

Fig. 1. Geologic map of the mid- to north-central Norway area of the Scandinavian Caledonides, modified after Solli (1995, 1999), Solli et al. (1997), and Braathen et al. (2002). The study area (Fig. 2) is indicated. Inset shows the regional context for the study area. Faults traces on the western margins of the basement windows, Børgefjellet, Nasafjället and Rombak, are approximate; the outlines and terminations of these faults have not yet been mapped in detail. CNBW = Central Norway basement window.

meyer 1998; Fossen & Dunlap 1998); 2) ductile extension and brittle reactivation in the Nordfjord-Sogn Detachment that juxtaposes footwall high-pressure metamorphic rocks against hanging-wall nappes and Devonian basins in southwest Norway (Andersen et al. 1998; Eide et al. 1999); and 3) extension and unroofing through a basement-nappe sequence in the Lofoten-Ofoten region of northern Norway (Fig. 1) (Coker et al. 1995; Hames & Andresen 1996; Northrup 1997). A common thread through these $^{40}Ar/^{39}Ar$ investigations has been the emphasis on the importance of extensional detachments and ductile shear zones in the syn- to

post-collisional evolution of the Scandinavian Caledonide mountain belt. In this vein, a picture emerging from numerous structural studies indicates the importance of a changing strain-field during the final throes of Siluro-Devonian continental collision and through the post-collisional phase. These studies reveal a pervasive top-W to top-SW ductile shear regime, present throughout various levels of the tectonostratigraphy, with different shear-transport directions identified in and allocated to specific corridors of the 1700-km long mountain chain (Roberts 1998; Krabbendam & Dewey 1998; Braathen et al. 2000, 2002; Osmundsen et al. 2003) (Fig. 1). A regionally prevalent system of ductile shear zones and extensional detachments has strong implications for the manner in which the mountain belt disintegrated during and following continental collision. Precise ages for the timing of activation/reactivation of the different shear zones and extensional detachments, coupled with kinematic analyses, as in this study, are prerequisite to understanding the shear systems within an evolving strain-field.

Kinematic analysis of the Nesna Shear Zone (NSZ) in Nordland, north-central Norway (Fig. 1), demonstrates that this shear zone, within the Uppermost Allochthon, contains a penetrative, top-WSW ductile fabric (Osmundsen et al. 2003). The fabric developed in a syn/post-collisional strain-field characterized generally by orogen-parallel extensional shearing coupled with shortening normal to the extension direction; the overall regime was probably one of sinistral transpression that developed into one of transtension (Braathen et al. 2002; Osmundsen et al. 2003). The NSZ has top-WSW, orogen-parallel fabrics similar to those identified in the Central Norway basement window (CNBW) to the south (Fig. 1) and represents a regional link between an 'orogen-parallel' shear system of probable Devonian age (Braathen et al. 2002; Osmundsen et al. 2003) and Silurian through latest Devonian top-W to top-NW ductile extension and unroofing defined for the Lofoten-Ofoten region to the north (Fig. 1) (Dallmeyer & Andresen 1992; Anderson et al. 1992; Coker et al. 1995; Northrup 1997; Klein et al. 1999). We conducted $^{40}Ar/^{39}Ar$ analyses on mica and K-feldspar from a sample profile through the NSZ and into the underlying Sjona window, a gneiss-cored culmination (Fig. 2), in order to constrain time and duration of extensional shearing in the NSZ and unroofing of its footwall. These data were used to evaluate the NSZ's role within the Mid Paleozoic strain-field of central through northern Norway during and following the waning phases of continental collision. Furthermore, the newly mapped continuations of the NSZ and the Kollstraumen detachment (KD) (Fig. 1) into the basement offshore Mid Norway (Olesen et al. 2002) raise important questions about the development of the deep structure of these offshore areas. Age and kinematic information from the onshore shear zones may provide first-order constraints for understanding the evolution of the offshore basement structures. A thorough kinematic analysis of the NSZ is presented in Osmundsen et al. (2003); we outline below only the main aspects of the structural/kinematic setting of the study region as it pertains to interpretation of the $^{40}Ar/^{39}Ar$ data. Throughout the paper we use the Devonian time scale as defined by Tucker et al. (1998).

Geologic setting and primary structural features

The rocks exposed today in the Scandinavian Caledonides preserve evidence for processes of rifting, arc-continent interaction, nappe emplacement and continental subduction and collision. These processes record the latest Precambrian separation of Baltica from a mega-continental assembly at high paleolatitudes, the early Paleozoic amalgamation of island-arcs and microcontinents to Baltica as several oceans opened and closed, and the destruction of Iapetus that culminated in subduction of Baltica beneath, and oblique collision with, Laurentia in Silurian-earliest Devonian time (Torsvik 1998; Eide & Lardeaux 2002; Cocks & Torsvik 2002). Allochthonous sheets were generally amalgamated and emplaced east- to southeastward (in present coordinates) onto the western Baltica margin, and have been subdivided into Lower, Middle, Upper and Uppermost Allochthons to correspond broadly with their emplacement order and their progressively more outboard derivations (Roberts & Gee 1985). The metamorphosed (par) autochthonous crust of Baltica is now exposed in a series of gneiss-cored culminations through the eroded nappe pile (Fig. 1).

North-central Norway (Figs. 1 and 2) is dominated by the exposed mass of the Uppermost Allochthon, which has a suggested Laurentian affinity (Roberts et al. 1985; Stephens & Gee 1985). The Uppermost Allochthon comprises a variety of ortho- and para-gneisses, marbles, amphibolites, ophiolite fragments and large volumes of granitic to gabbroic rocks (Stephens et al. 1985; Nordgulen et al. 1993; Yoshinobu et al. 2002). In the Nesna area (Fig. 2), the Uppermost Allochthon is represented by the Helgeland Nappe Complex (HNC), with large volumes of granitic to gabbroic intrusive complexes and minor calc-silicates, marbles and ophiolite fragments, and the underlying Rödingsfjäll Nappe Complex (RNC), which consists of schists and gneisses with interleaved marbles. The NSZ forms the lower boundary of the HNC, and in the Nesna area, the NSZ thins and partly excises the uppermost RNC along this lower, sheared HNC contact (Fig. 2); to the south, the entire RNC is excised in the footwall of the NSZ. Although kyanite-bearing assemblages occur in both the HNC and RNC, indicating early, upper amphibolite- to

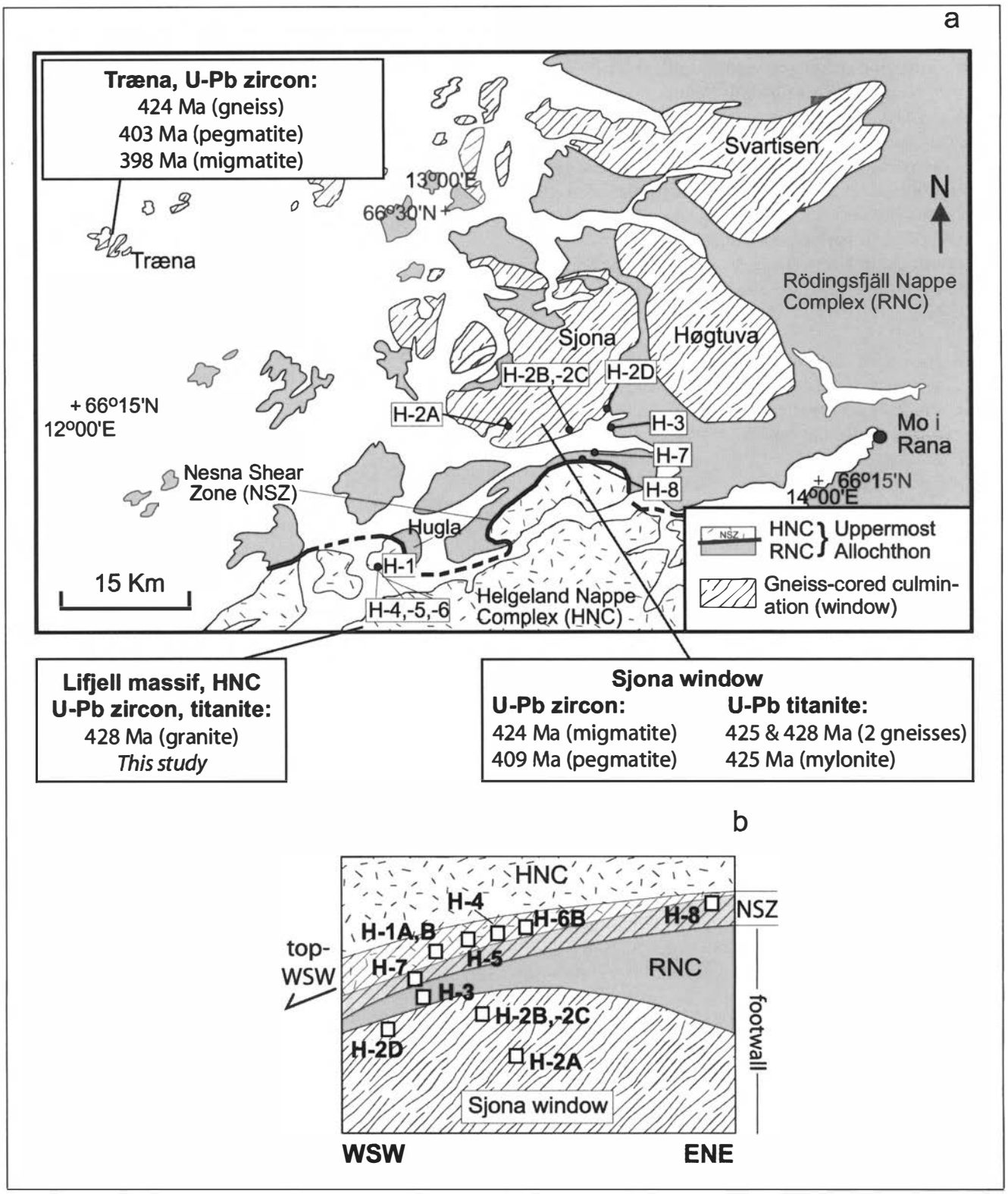

Fig. 2. Geology and tectonostratigraphy of the Nesna area and $^{40}Ar/^{39}Ar$ sample localities. a) Primary geologic units include the gneiss-cored culminations (Sjona, Høgtuva, and Svartisen windows) and the Træna gneisses, overlain by the Uppermost Allochthon units which here comprise the Rödingsfjäll Nappe Complex (RNC) and the Helgeland Nappe Complex (HNC). The Nesna Shear Zone (NSZ) in this area generally follows the boundary between the RNC and HNC, but also partially excises the uppermost RNC (see also (b)). U-Pb ages from Træna and Sjona gneisses (Larsen et al. 2002) and the Lifjell granite in the HNC (this study) are indicated. $^{40}Ar/^{39}Ar$ sample localities are identified in white boxes (see relative tectonostratigraphic positions in (b)). b) Schematic representation of the local tectonostratigraphy with approximate sampling levels. The NSZ is a c. 1 km thick shear zone with dominant top-WSW fabric. The NSZ is generally subparallel to the contact between the HNC and RNC, but we note that the shear zone varies in thickness, is folded and cuts downward through the tectonostratigraphic section. Part of the RNC and the Sjona window, a gneiss-cored culmination, are thus in the footwall of the NSZ. Sample H-8 is the highest level of the NSZ sampled in this study and derives from the uppermost unit of the RNC, at the HNC contact.

low-P granulite-facies metamorphism, these nappes in the Nesna area now contain mineral assemblages predominantly indicative of amphibolite- to upper greenschist- facies metamorphic conditions.

Immediately north of the NSZ, exposed in culminations through the eroded RNC, are several gneiss-cored culminations, the largest of which are the Sjona, Høgtuva and Svartisen windows (Figs. 1 and 2). These domes comprise granitic and migmatitic gneisses of dominantly amphibolite- to upper greenschist-facies metamorphic grade, although on the island of Træna, severely retrogressed eclogites of unknown age are preserved as lenses within the gneissic basement (Fig. 2; Gustavson & Gjelle 1991; Larsen et al. 2002).

The structural fabrics in the Nesna region, from the gneiss-cored culminations, upsection through the RNC and into the NSZ, can be summarized as follows: Folds, fold-trains, lineations and S-C fabrics in the footwall of the NSZ, including gneisses in the Træna and Sjona areas, and the RNC exposed beneath the NSZ, preserve a top-ENE transport direction interpreted to record early thrusting and nappe emplacement, probably near the onset of continental collision (Larsen et al. 2002; Osmundsen et al. 2003). The gneissose foliation of the RNC wraps the Sjona and Høgtuva windows in a somewhat complex fashion: the foliation contains both top-NW backfolds and, particularly around the Sjona window, a radially distributed, down-dip lineation. These fabrics post-date the top-ENE thrust-related fabrics and are suggested to have evolved during doming/unroofing of the gneiss-cored culminations (Larsen et al. 2002; Osmundsen et al. 2003). Farther upward in the RNC and with closer proximity to the NSZ, relict, top-ENE thrust-related fabrics become progressively overprinted by SW-dipping shear bands and top-SW lineations. The NSZ itself comprises a ca. 1 km-thick zone of S>L tectonites dominated by SW- to W-dipping shear bands and an ENE-WSW-oriented stretching lineation often defined by retrograde biotite wrapping garnet porphyroclasts (Osmundsen et al. 2003). On a regional scale (Fig. 1) the NSZ and HNC are folded into a large, open synform (with gently plunging axis oriented 235°) interpreted to have developed during extension-parallel folding (Osmundsen et al. 2003; Braathen et al. 2002).

Importantly, several gneiss-cored culminations exposed immediately east and northeast of the Uppermost Allochthon (the Børgefjell and Nasafjäll windows, Fig. 1) are bounded by top-WSW, relatively steeply dipping, ductile- to brittle- extensional shear zones. These 150 to 500 m-thick shear zones developed under greenschist-facies and lower conditions and dramatically thin or excise the Middle and Upper Allochthons through which they cut. Osmundsen et al. (2003) have suggested that these steeply-dipping structures can be correlated with a similar feature farther north, on the west margin of the Rombak window (Fig. 1) (Rykkelid & Andresen 1994), of probable Late Devonian age (Coates et al. 1999), and have further proposed that all of these steep faults, including the NE-dipping Kollstraumen detachment, overlap and post-date activity on the NSZ (see also Braathen et al. 2000, 2002).

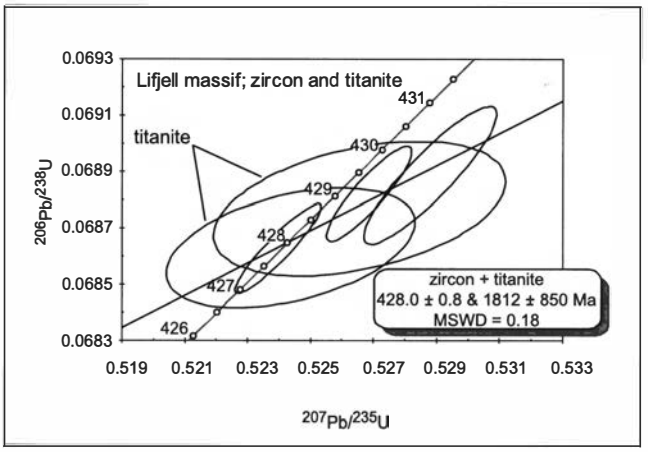

Fig. 3. U-Pb concordia diagram from three zircons and two titanites from the Lifjell massif. Ages overlap within uncertainty and yield a crystallization age for the massif of 428.0 ± 0.8 Ma. The upper intercept suggests an inherited Proterozoic component. See Appendix for analytical protocol.

Other geochronology, Nesna area

U-Pb ages from gneisses in the NSZ footwall and a new U-Pb age from a HNC granite dated in this study, directly above the NSZ, have provided primary ties for interpretation of our $^{40}Ar/^{39}Ar$ data. From the Sjona window, Larsen et al. (2002) report U-Pb zircon lower intercept ages of 424 ± 14 Ma for a migmatitic gneiss, U-Pb titanite ages of 425 ± 3 Ma and 428 ± 3 Ma for amphibolite-facies gneisses and a U-Pb titanite age from top-E mylonite of 425 ± 2 Ma. A pegmatite cross-cutting the Sjona gneissic foliation yielded a U-Pb zircon upper intercept age of 409 ± 5 Ma (Fig. 2). On Træna, a similar age distribution occurs: U-Pb titanite ages of 424 ± 6 Ma (gneiss), 398 ± 2 Ma (migmatite) and 403 ± 3 Ma (discordant pegmatite) are reported (Larsen et al. 2002). The 424-428 Ma ages are interpreted to date the time of amphibolite facies metamorphism and partial melting of the gneisses, probably related to Siluro-Devonian collision and thrusting; the 398-409 Ma ages are linked to decompression melting and doming of the gneissic units (Larsen et al. 2002).

To bracket the hanging-wall age of the NSZ, we conducted U-Pb analyses by TIMS (thermal ionization mass spectrometry; see Appendix for analytical protocol) on a porphyritic granodiorite from the Lifjell massif of the HNC (Figs. 1 and 2). The Lifjell massif has a

Table 1. U-Pb data for Lifjell Massif porphyritic granodiorite (GBM.NL.9922)

Mineral, characteristics	Weight	U	Th/U	Pbc		$^{206}Pb/^{204}Pb$	$^{207}Pb/^{235}U$	2σ	$^{206}Pb/^{238}U$	2σ	rho	$^{207}Pb/^{206}Pb$	2σ	$^{207}Pb/^{235}U$	$^{206}Pb/^{238}U$	$^{207}Pb/^{206}Pb$
	[µg]	[ppm]		[ppm]	[pg]			[abs]		[abs]			[abs]	[Ma]		
(1)	(1)	(2)	(3)	(4)	(4)	(5)	(6)	(6)	(6)	(6)		(6)	(6)	(6)	(6)	(6)
Z tips eu-sb	21	558	0.47		4.2	12161	0.5269	11	0.06882	14	0.89	0.05552	5	429.1	429.7	433.3
Z eu-sb sp	36	768	0.46		5.6	21417	0.5288	17	0.06889	20	0.90	0.05567	8	429.4	431.0	439.4
Z tips eu-sb	27	807	0.46		12	7609	0.5240	11	0.06863	13	0.93	0.05537	4	427.9	427.8	427.4
T br-rd fr	335	432	1.12	3.5		548	0.5244	32	0.06863	17	0.43	0.05541	31	427.9	428.1	429.0
T br-rd fr large	245	408	0.92	3.9		470	0.5265	38	0.06877	20	0.40	0.05553	37	428.7	429.5	433.7

(1) Z = zircon; T = titanite; eu = euhedral; sb = subhedral; sp = short prismatic (l/w = 2-4); fr = fragment; br = brown; rd = red
(2,4) weight and concentrations are known to better than 10%
(3) Th/U model ratio inferred from 208/206 ratio and age of sample
(4) Pbc = total common Pb in sample (initial +blank)
(5) raw data corrected for fractionation and blank
(6) corrected for fractionation, spike, blank and initial common Pb (calculated with Stacey and Kramers (1975) model; the errors were calculated by propagating the main sources of uncertainty; errors indicate the last significant digits of the values

relatively undeformed interior and a pronounced foliation on its northern margin, subparallel to the NSZ fabrics. Orientation of shear fabrics on the massif margin indicates that the edge of the granodiorite was affected by the same top-WSW deformation as that observed within the NSZ. U-Pb zircon and titanite analyses from the relatively undeformed interior of the massif yielded concordant to slightly discordant zircons with a slight suggestion of Proterozoic inheritance; the titanites are concordant and overlap the zircon data. The data together yield an age of 428.0 ± 0.8 Ma (Table 1; Fig. 3) that we interpret to represent crystallization of the granodiorite and a maximum age for deformation on the NSZ.

Dallmeyer (1988), who referred to unpublished hornblende ages between 401 and 418 Ma from the Sjona and Høgtuva windows, described the only previous $^{40}Ar/^{39}Ar$ ages from the Nesna vicinity. Adhering to nominal closure temperatures for amphibole (500 ± 25°C; Harrison 1981) and biotite (ca. 300-350°C; McDougall & Harrison 1999), the reported amphibole ages provide an upper limit for the biotite ages we obtained from the Sjona window (see below).

Nesna Shear Zone profile

A primary objective of our study was to obtain $^{40}Ar/^{39}Ar$ age information that could be directly linked to ductile, top-WSW shearing in the NSZ, and unroofing of its footwall. We sampled in a profile through the NSZ and its footwall, focusing on localities where we have control on structural fabrics (see Osmundsen et al. 2003) (Fig. 2).

Footwall samples

Five footwall samples, four from an interior-to-margin profile through the Sjona window and one from the RNC, below the NSZ, were selected for $^{40}Ar/^{39}Ar$ analysis (Fig. 2). The Sjona window samples comprise granitic to granodioritic gneisses (H-2A, H-2B), a granitic protomylonite sample H–2D, and a discordant, coarse-grained pegmatite (H-2C) that cuts H-2B. The gneissic foliation becomes more pronounced toward the eastern margin of the Sjona window, with the strongest fabric development in protomylonite sample H-2D. The primary mineral assemblage in the Sjona samples includes biotite, quartz, K-feldspar, plagioclase and oxides; sample H–2C contains additional epidote and hornblende. Sample H-3 from the RNC, above the Sjona window and below the NSZ, is a coarse-grained plagioclase-quartz-garnet-biotite gneiss. Minor biotite and/or chlorite replacement is evident on garnet rims; retrograde chlorite is also weakly developed on some matrix biotite. The gneiss fabric in sample H-3 contains some top-WSW shear-sense indicators, but the sample derives from below what we determine to be the main NSZ. We conducted $^{40}Ar/^{39}Ar$ analyses on biotite from sample H-3, and biotite and K-feldspar from samples H-2A, H-2B, H-2C, and H–2D, with an additional hornblende analysis from pegmatite H-2C.

Nesna Shear Zone samples

Seven NSZ samples, five from the lowermost HNC and two from the uppermost RNC, were analyzed (Fig. 2). The five HNC samples derive from different gneiss lithologies on the island of Hugla (Fig. 2) and include a quartz-white mica gneiss (H-1A), a garnet-feldspar-biotite gneiss (H-1B), a garnet-kyanite-white mica-bio-

Table 2. Summary table of $^{40}Ar/^{39}Ar$ data

Sample	Mineral	Rock	TFA (Ma)	Weighted mean age (Ma)	Simple mean age (Ma)	Steps used/ (%^{39}Ar)[1]	Inverse isochron age (Ma)	$^{40}Ar/^{36}Ar$ intercept	SUMS/ (n-2)2	Age (Ma) with J-value uncertainty
Footwall samples										
Sjona window										
H-2A	biotite	granitic gneiss	379.0 ± 0.2	384.8 ± 0.1	384.7 ± 2.8	4-12/ (43.5)	**384.3 ± 1.0**	293.8 ± 5.3	5.4	384.3 ± 3.5
H-2A	K-feldspar	granitic gneiss	333.3 ± 0.2	not used	**342 ± 7**	6-10/ (49.1)	not calculated	--	--	342 ± 7
H-2B	biotite	granitic gneiss	387.5 ± 0.1	389.0 ± 0.1	389.1 ± 1.6	4-15/ (84.6)	**389.3 ± 0.8**	284.6 ± 17.6	5.5	385.0 ± 3.9
H-2B	K-feldspar	granitic gneiss	324.5 ± 0.3	not used	**336 ± 8**	19-28/ (61.2)	not calculated	--	--	336 ± 9
H-2C	K-feldspar	pegmatite	340.1 ± 0.3	not used	**346 ± 14**	21-31/ (58.4)	not calculated	--	--	346 ± 14
H-2D	biotite	granitic protomylonite	377.5 ± 0.2	378.1 ± 0.1	378.8 ± 4.2	3-15/ (96.9)	**378.3 ± 0.9**	302.7 ± 6.2	20.7	378.3 ± 3.4
H-2D	K-feldspar	granitic protomylonite	312.4 ± 0.3	not used	**335 ± 6**	18-27/ (38.3)	not calculated	--	--	335 ± 6
Rødingsfjell Nappe Complex										
H-3	biotite	Pl-Qz-Gt-Bi gneiss	378.8 ± 0.1	382.6 ± 0.1	383.2 ± 2.4	4-20/ (93.5)	**382.8 ± 0.6**	303.2 ± 10.6	23.2	382.8 ± 3.4
Nesna Shear Zone samples										
Helgeland Nappe Complex										
H-1A	white mica	Qz-Wm gneiss	394.3 ± 0.2	392.0 ± 0.1	391.4 ± 2.7	7-13/ (84.0)	**392.8 ± 2.2**	256.8 ± 40.0	15.4	392.0 ± 3.4
H-6B	white mica	Gt-Qtz-Pl-Wm-Ky-Bi gneiss	390.0 ± 0.2	393.8 ± 0.1	394.9 ± 4.5	5-11/ (63.7)	**390.1 ± 1.7**	325.3 ± 16.3	11.1	390.1 ± 3.8
H-4	white mica	Gt-Ky-Wm-Bi gneiss	395.6 ± 0.1	396.6 ± 0.1	396.8 ± 3.1	4-17/ (89.9)	**393.8 ± 1.2**	329.1 ± 14.8	14.2	393.8 ± 3.6
H-5	white mica	Qz-Pl-Gt-Wm gneiss	384.9 ± 0.1	389.5 ± 0.1	390.1 ± 2.5	7-12 & 18-20/ (63.9)	**389.0 ± 1.3**	301.9 ± 20.5	8.3	389.0 ± 3.6
H-1B	biotite	Gt-Fsp-Bi gneiss	388.4 ± 0.1	388.6 ± 0.1	392.0 ± 5.9	4-14/ (92.4)	**387.6 ± 1.4**	337.3 ± 22.2	60.2	387.6 ± 3.6
Rödingsfjäll Nappe Complex										
H-7	biotite	Qz-Fsp-Bi gneiss	385.8 ± 0.2	387.1 ± 0.1	386.3 ± 2.2	4-17/ (96.1)	**387.1 ± 0.8**	290.3 ± 9.2	20.3	387.1 ± 3.4
H-8	biotite	marble	397.3 ± 0.1	398.2 ± 0.1	399.2 ± 4.2	3-17/ (97.7)	**397.8 ± 1.0**	291.7 ± 12.2	29.7	397.8 ± 3.6

Biotite (Bi), white mica (Wm) and K-feldspar (Ksp) were analyzed by step-heating with a resistance furnace. Uncertainties in ages are cited at 1s without error in J-value (all samples irradiated together), except for the final column (right-hand side) where the age is cited at 1s with J-value uncertainty to facilitate comparison to other published age data. Errors for isochron ages are standard errors. Ages in bold are those used in text and regional interpretation. -- = no value (because no isochron calculated). Other mineral abbreviations: Qz = Quartz, Gt = Garnet, Pl = Plagioclase, Ky = Kyanite, Fsp = feldspar (undifferentiated)

(1) 'Steps used' refers to the step numbers (usually consecutive) used in the weighted-mean age calculation. These steps correspond to the same steps in release spectrum diagrams (Figs. 4-7) and in the data tables in Appendix 2. %^{39}Ar = the percentage of cumulative ^{39}Ar gas represented by the indicated steps.

(2) Relatively high SUMS/(n-2) compared to apparent spread of $^{40}Ar/^{36}Ar$ ratios in isochron diagrams (Figs. 4-7) are due to very small uncertainties on individual data points.

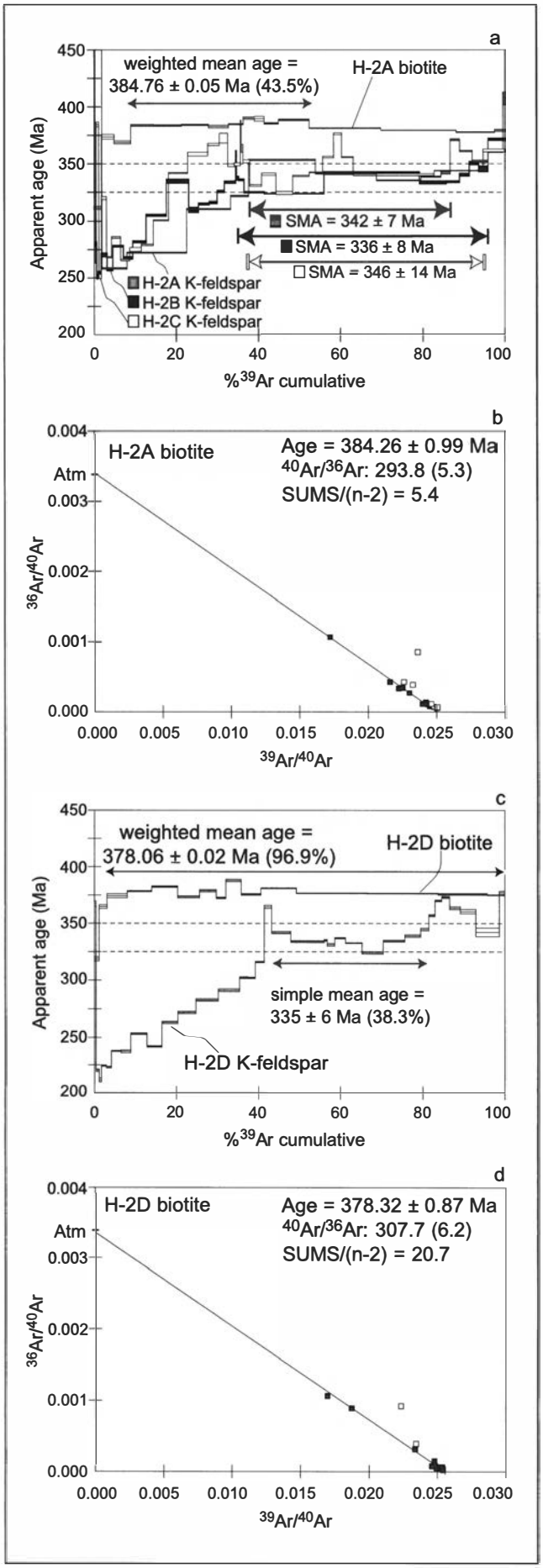

tite gneiss (H-4), a quartz-plagioclase-garnet-white mica gneiss (H-5), and a garnet-quartz-plagioclase-white mica-kyanite-biotite gneiss (H-6B) (see also Table 2). All of these samples have a penetrative, composite top-WSW fabric with ENE–WSW-oriented stretching lineations and W-verging shear bands, particularly prominent in garnet-biotite-white mica gneisses (Osmundsen et al. 2003). White mica from H-1A, H-4, H-5 and H-6B were separated for $^{40}Ar/^{39}Ar$ analysis. Biotite from H-1B was also analyzed.

The two samples from the uppermost RNC derive from two different structural levels of the attenuated section within the NSZ (Fig. 2). Sample H-7, a quartzo-feldspathic gneiss with biotite, was taken from the lowest structural level of the NSZ. Sample H-8, a coarsely crystalline marble with biotite, was taken from the uppermost unit in the RNC—at the contact with the base of the HNC—and from the highest structural level of the NSZ that we sampled. The RNC marbles at this contact are spectacularly deformed into west-verging fold trains and it appears that the shear zone was, in part, lubricated by the highly ductile marbles along this contact (Osmundsen et al. 2003). Biotite was analyzed from both H-7 and H–8.

$^{40}Ar/^{39}Ar$ geochronology

Analytical protocol

The analyses were performed at the $^{40}Ar/^{39}Ar$ geochronology laboratory at the Geological Survey of Norway. Gas was extracted from all samples by resistance-fur-

Fig. 4. $^{40}Ar/^{39}Ar$ release spectra and inverse isochron diagrams for footwall biotites and K-feldspars. Weighted-mean ages from release spectra incorporate individual steps weighted according to both amount of ^{39}Ar and uncertainty in the apparent age. SMA = simple mean age (calculated without weighting for amount of ^{39}Ar). In inverse isochron diagrams, poor fit of a line to the data (SUMS/(n-2) > 2.5) indicates greater uncertainty than that attributable to analytical error alone. Uncertainties on individual data points in isochron diagrams are plotted on the figures, and are usually smaller than the data point. Black data points were those used in the regression and represent the same steps as those used in the weighted-mean age calculations; white data points were excluded from the regression (see Table 2).

a) Release spectra for footwall biotite H-2A and K-feldspars H-2A, H-2B and H-2C. Weighted-mean age for biotite and simple-mean ages for K-feldspars are discussed in the text. Simple mean ages calculated for the central segments of the K-feldspar release spectra have larger errors than corresponding weighted-mean ages and better reflect the variability of the irregular gas-release patterns. Dashed lines are added at 325 and 350 Ma as visual aids.

b) Inverse isochron diagram for biotite from H-2A. See text and Table 2 for details.

c) Release spectra for footwall biotite H-2D and K-feldspar H-2D. Data presented as in (a).

d) Inverse isochron diagram for biotite H-2D. Data presented as in (b).

nace step-heating. Analytical data are presented in Table 2 and in Figures 4-7. In the following descriptions, figures, and tables, ages are cited at 1 σ uncertainty *without* intralaboratory uncertainty in J-value (1%) (all samples were included in the same irradiation package). Ages in the last column of Table 2 are cited at 1 σ uncertainty *with* J-value uncertainty to facilitate comparison to other published studies. Detailed analytical procedures and complete data tables are presented in the Appendix.

Data

Footwall biotites - Age spectrum and inverse isochron plots for biotite samples from the NSZ footwall are plotted in Figures 4 and 5. Weighted-mean ages for biotites, comprising between 44 and 97% of the total gas released in the experiments, have been determined for the most concordant parts of the release spectra (Figs. 4a, 4c and 5a). In inverse isochron diagrams, ages determined from regressions through the same steps used in the weighted-mean calculations are within error of the weighted-mean ages and yield near-atmosphere, trapped $^{40}Ar/^{36}Ar$ components (Figs. 4b, 4d, 5b and 5c; Table 2). Isochron ages are used in later discussion of the samples.

The release spectrum for biotite H-2A yielded a set of steps corresponding to a weighted-mean age of 384.76 ± 0.05 Ma (Fig. 4a, upper spectrum) and an inverse isochron age of 384.26 ± 0.99 Ma (Fig. 4b). The 15-step release spectrum for biotite H-2D protomylonite yielded a weighted-mean age of 378.06 ± 0.02 Ma (Fig. 4c, upper spectrum) and an inverse isochron age of 378.32 ± 0.87 Ma (Fig. 4d). The release spectrum for biotite H-2B yielded a set of steps corresponding to a weighted-mean age of 389.03 ± 0.02 Ma (Fig. 5a, upper spectrum). On an inverse isochron, the data define a linear array with a $^{40}Ar/^{39}Ar$ intercept corresponding to an age of 389.29 ± 0.77 Ma (Fig. 5b). Seventeen of 20 steps in the release spectrum for biotite H-3 are reasonably concordant and correspond to a weighted-mean age of 382.57 ± 0.01 Ma (Fig. 5a, lower spectrum). The same steps on an inverse isochron correspond to an age of 382.80 ± 0.56 Ma (Fig. 5c).

Footwall feldspars - The feldspars from the Sjona gneiss window yield similar gas-release patterns, regardless the degree of sample deformation (compare protomylonite H-2D to relatively weakly deformed pegmatite H-2C; Figs. 4a and 4c). Apparent ages climb from ca. 225-260 Ma to ca. 325-350 Ma within the first 30-40% of gas released in the experiments. The apparent ages for the subsequent ca. 30-50% of the experiments vary between 325 and 350 Ma. Imprecise, simple mean ages between 335 ± 6 and 346 ± 14 Ma characterize these latter portions of the four spectra. The gas released at high experimental temperatures yields a series of low-

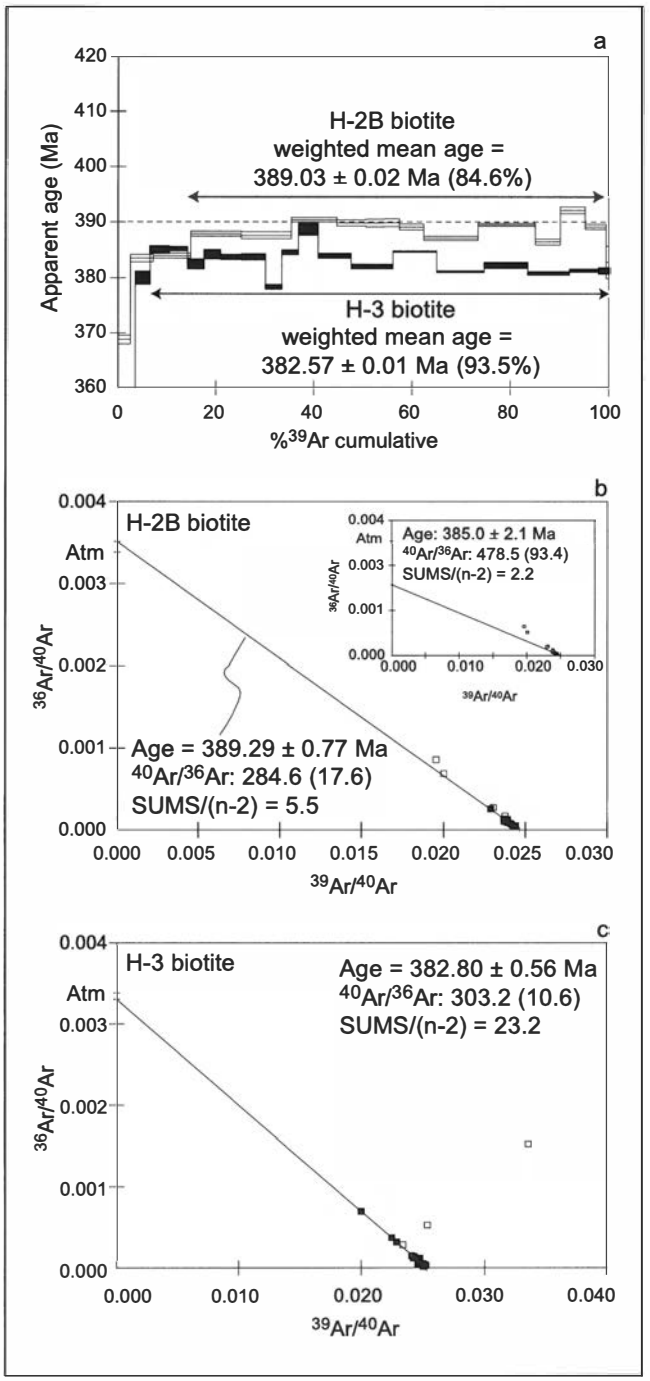

Fig. 5. $^{40}Ar/^{39}Ar$ data from footwall biotites H-2B and H-3. Data presented as in Figure 4.
a) Release spectra for the two samples. Dashed line added at 390 Ma as visual aid.
b) Inverse isochron diagram for biotite H-2B. Primary isochron calculated using the same steps used in the weighted-mean age calculation yields an age of 389.3 ± 0.8 Ma. Inset shows a regression through only the steps with highest radiogenic ^{40}Ar yield (Steps 6 through 12, Appendix 2); a younger age of 385 ± 2 Ma is calculated, with an age similar within uncertainty to footwall biotites H-2A and H-3. Although this alternative regression has a $^{40}Ar/^{36}Ar$ ratio greater than atmosphere and hints that the older age of ca. 389 Ma may have been affected by excess ^{40}Ar, we have no compelling reason to exclude the slightly less radiogenic steps 4, 5, and 13-15 from the regression and conservatively use the older age of 389 Ma for this sample.
c) Inverse isochron diagram for biotite H-3.

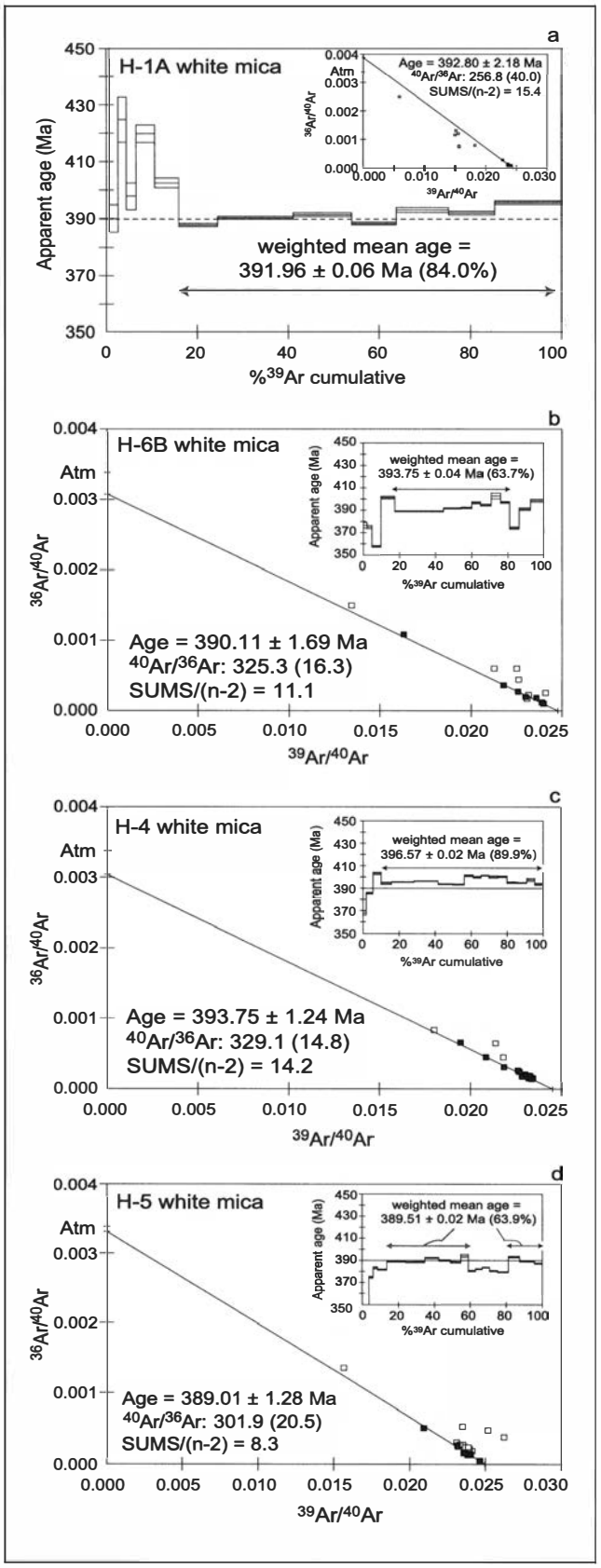

Fig. 6. $^{40}Ar/^{39}Ar$ data for white mica and biotite from the HNC within the NSZ. Data presented as in Figure 4.
a) Release spectrum for white mica H-1A with inverse isochron inset.
b) Inverse isochron for white mica H-6B with release spectrum inset.
c) Inverse isochron for white mica H-4 with release spectrum inset.
d) Inverse isochron for white mica H-5 with release spectrum inset.

volume steps with irregularly increasing apparent ages that vary between ca. 350 and 370 Ma, approaching the apparent ages in the biotite spectra. Minor excursions toward 370 Ma ages are also evident in the middle of the experiment for feldspar H-2C (Fig. 4a).

Summary, footwall samples - The total age variation for the biotite samples is between 378.3 ± 0.9 Ma (H-2D, Sjona protomylonite) and 389.3 ± 0.8 Ma (H-2B, granitic gneiss, Sjona interior) that we interpret to represent the times of closure of the biotites to argon loss. Biotite samples H-2A and H-3 have ages within uncertainty of one another and we presume these biotites closed to argon loss at about the same time and temperature (between ca. 300 and 350°C). The statistically younger cooling age from H-2D protomylonite is interpreted to document the time of formation of the mylonitic fabric—which slightly post-dated cooling in other parts of the footwall.

In the feldspar samples, the small excursions in the spectra toward 370 Ma ages are interpreted to represent a relict cooling age-signature from a very retentive portion of the feldspars; 370 Ma cooling ages would have succeeded reasonably closely upon the 378-389 Ma ages that characterize closure to argon in biotites from the same rocks. Simple mean ages between 335 and 346 Ma for steps comprising the majority of gas released in all of the feldspar experiments are interpreted to record a separate and geologically meaningful portion of the K-feldspar cooling histories. Preliminary multi-domain diffusion (MDD) modeling on the two feldspars for which we used isothermal, cycled heating schedules suggests rapid cooling between ca. 350 and 330 Ma (see Eide et al. 1999 for discussion of MDD modeling procedures used). The decrease in apparent ages from this Early Carboniferous signature toward apparent ages of ca. 220-260 Ma registered at the start of the experiments may be attributed to partial argon loss, resumption of slow cooling, or a combination of these.

Both biotite and hornblende from pegmatite sample H-2C yielded complicated gas-release patterns with gas apparently liberated from several reservoirs in each mineral, complicated by excess argon components. No geologically interpretable ages were obtained from these samples.

Nesna Shear Zone white micas – Age spectrum and inverse isochron plots for white mica samples (H-1A, H-6B, H-4 and H-5) from the HNC within the NSZ are plotted in Figure 6. Weighted-mean ages have been determined for the most concordant parts of the release spectra, although some spectra exhibit marked discordance over as much as 20% of the experiment (Fig. 6b, c and d). The variability within the spectra is assessed through inverse isochron diagrams. Regressions for two samples, H-1A and H-5, yield an atmospheric $^{40}Ar/^{36}Ar$

intercept and a $^{40}Ar/^{39}Ar$ intercept within error of the weighted-mean ages (Figs. 6a, d; Table 2). The other two samples, H-6B and H-4, yield $^{40}Ar/^{39}Ar$ intercept ages younger than weighted-mean ages with $^{40}Ar/^{36}Ar$ intercepts indicating trapped components of non-atmospheric value (Figs. 6b, c; Table 2). Isochron ages are used in later discussion of the samples (Table 2).

The release spectrum for white mica H-1A yielded a set of steps corresponding to a weighted-mean age of 391.96 ± 0.06 Ma and an inverse isochron age of 392.80 ± 2.18 Ma (Fig. 6a). The release spectrum from white mica H-6B yielded a weighted-mean age of 393.75 ± 0.04 Ma. The same data on an inverse isochron yielded age of 390.11 ± 1.69 Ma with a trapped argon composition greater than atmospheric value (Fig. 6b; Table 2).

The release spectrum for white mica H-4 yields a set of 14 semi-concordant steps with a weighted-mean age of 396.57 ± 0.02 Ma and an inverse isochron age of 393.75 ± 1.24 Ma, slightly younger than the weighted-mean age, with a trapped argon ratio above atmospheric value (Fig. 6c). The release spectrum from white mica H-5 yields a weighted-mean age of 389.51 ± 0.02 Ma for ca. 64% of the experiment and an inverse isochron age of 389.01 ± 1.28 Ma (Fig. 6d). However, the spectrum pattern is complicated by an internally concordant region comprising about 20% of the experiment with a significantly lower apparent age of ca. 382 Ma. These anomalous steps have lower radiogenic ^{40}Ar yields and lie on a different trend within the inverse isochron diagram, suggesting possible presence of a second mica phase in this sample (Appendix 2; Fig. 6d). We use the isochron age of 389.0 ± 1.3 Ma in the subsequent discussion; this age has larger uncertainty than the weighted-mean age and is considered more representative of the true variation observed in the sample.

Nesna Shear Zone biotites - Age spectrum and inverse isochron plots for biotite samples H-1B (HNC) and H-7 and H-8 (RNC) within the NSZ are plotted in Figure 7. A discordant spectrum for H-1B and very poor correlation of the data on an inverse isochron diagram suggests an age of 388 ± 1 Ma for the sample (Fig. 7a; Table 2). Biotites H-7 and H-8 yielded semi-concordant release spectra with weighted-mean ages of 387.11 ± 0.02 Ma and 398.17 ± 0.02 Ma, respectively (Fig. 7b; Table 2). Inverse isochron ages of 387.05 ± 0.78 Ma (H-7, Fig. 7c) and 397.83 ± 1.03 Ma (H-8, Fig. 7d) are within uncertainty of weighted-mean ages and correspond to atmospheric trapped $^{40}Ar/^{36}Ar$ components.

Summary, Nesna Shear Zone samples - The four white mica samples from within the HNC, in the central part of the NSZ, have a total age variation between 389.0 ± 1.3 Ma (H-5) and 393.8 ± 1.2 Ma (H-4), interpreted to correspond to time of closure to argon loss in the white micas. Biotite sample H-1B yielded an age of 388 ± 1

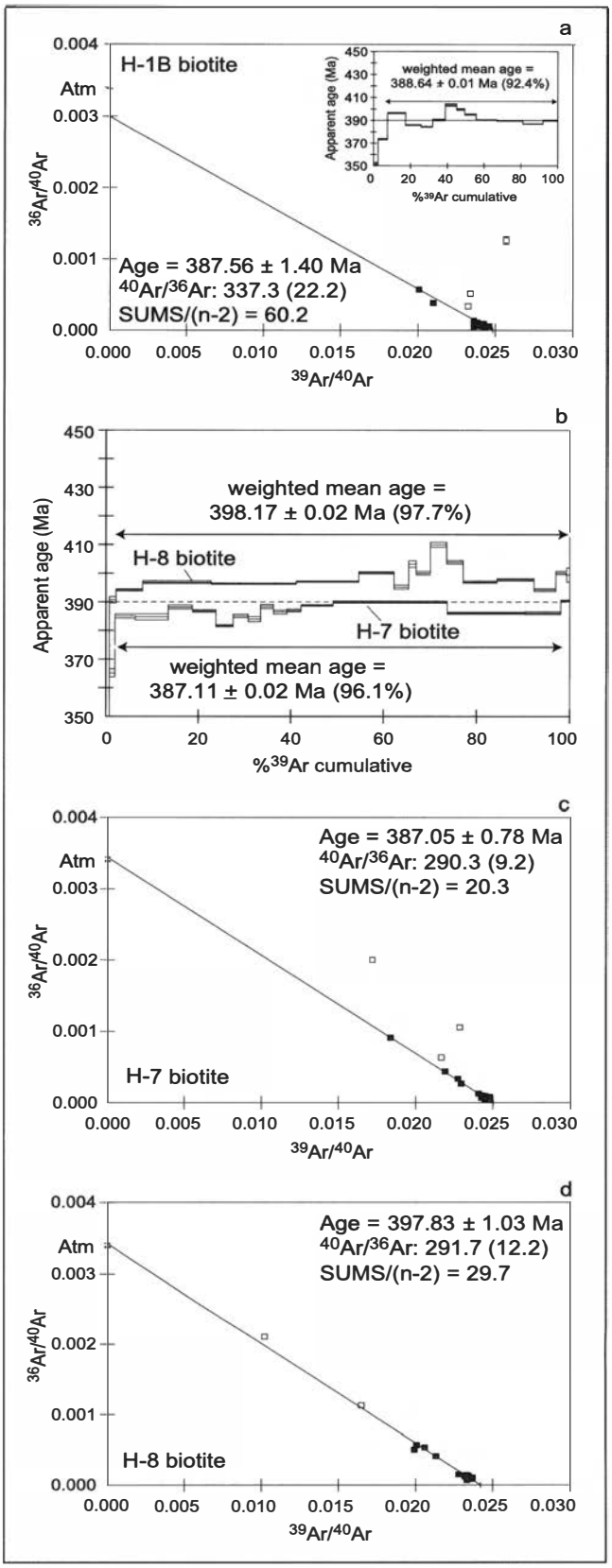

Fig. 7. $^{40}Ar/^{39}Ar$ data from biotites from the HNC (H-1B) and RNC (H-7, H-8) within the NSZ. Data presented as in Figure 4.
a) Inverse isochron for biotite H-1B with release spectrum inset.
b) Release spectra for RNC biotites H-7 and H-8. Dashed line at 390 Ma is visual aid.
c) Inverse isochron diagram for biotite H-7.
d) Inverse isochron diagram for biotite H-8.

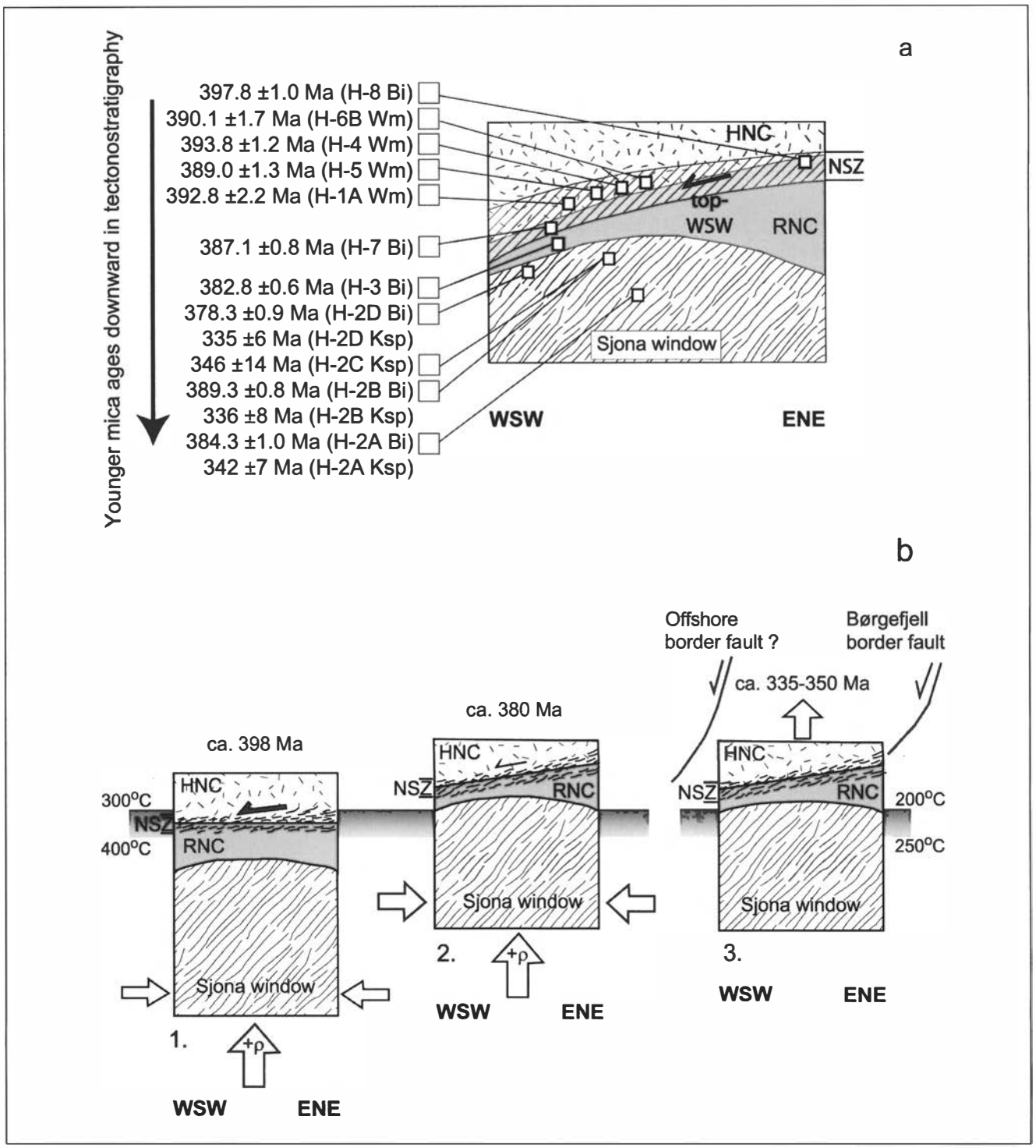

Fig. 8. Summary diagram showing:
a) Schematic tectonostratigraphy of Figure 2 with $^{40}Ar/^{39}Ar$ ages from this study. Bi = biotite; Wm = white mica; Ksp = K-feldspar.
b) Schematic diagram illustrating the time-progress of deformation on the NSZ relative to two phases of unroofing. The gray, shaded horizontal bar represents approximate crustal temperature (no depth indicated) for each time interval based on nominal Ar-closure temperatures for micas. Sizes of the block- and line- arrows indicate relative intensity of the crustal motion (unroofing or ductile shear) and its orientation. West-southwest is to the left in all of the figures. 1. Initiation of top-WSW motion on the NSZ at 398 Ma. The NSZ initiated along or near the contact between the HNC and RNC in a regime of orogen-parallel extension (middle-upper crust) accompanied at deep crustal levels by orogen-normal convergence. Net motion on the basement window is upward and results from a combination of convergence, positive buoyancy and upper crustal extension. Micas in the NSZ crystallized through temperatures of ca. 300-400°C. 2. Activity waned on the NSZ by ca. 380 Ma. The NSZ footwall rocks (biotites) pass through the same (fixed) geotherm indicated in (1) as unroofing continues. 3. Activation of the steeply dipping, ductile-to-brittle border faults along the west margins of the basement culminations by ca. 335-350 Ma. These faults re-used and crosscut older, low-angle shear zones like the NSZ and generated a situation favorable for continued footwall uplift. The feldspars of the Sjona window passed through temperatures of ca. 200-250°C at 335-350 Ma in this representation. The presence of an offshore, steeply dipping border fault is also proposed.

Ma, slightly younger than the age of white mica from the adjacent gneiss sample H-1A (392.8 ± 2.2 Ma).

The two biotites from the RNC within the NSZ (H7 and H8) represent the uppermost and lowermost levels of the shear zone sampled in this study and yielded two statistically distinct ages: 387.1 ± 0.8 Ma for the structurally lower sample and 397.8 ± 1.0 Ma for the marble sample at the uppermost RNC contact with the HNC. We interpret both ages to represent real, and different, times of closure to argon loss in the biotite samples. The biotites in the RNC bracket the complete range of activity within the NSZ in the Nesna area. The data indicate that the upper part of the NSZ was active in a ductile shear regime as early as 398 Ma and that this activity continued through at least 387 Ma. This youngest age obtained from biotite within the NSZ overlaps the oldest biotite age from the footwall (389 Ma, sample H-2B, Sjona window interior). However, the majority of the NSZ samples are significantly older (387-398 Ma) than the majority of the footwall samples (379-389 Ma). These data are summarized in Figure 8a and we discuss the significance of the ages within a tectonostratigraphic framework in the following section.

Discussion

The $^{40}Ar/^{39}Ar$ mica ages from a profile through the NSZ and its footwall decrease progressively downward through the tectonostratigraphy from 397.8 ± 1.0 to 378.3 ± 0.9 Ma (Fig. 8a). We interpret this downward-younging age pattern most broadly in terms of differential cooling and closure of the micas to argon loss as the crustal section was unroofed. When considering only intralaboratory uncertainties, the mica ages can further be divided into two groups, distinguished both on the basis of their statistical differences and the structural fabrics they represent. The first age group consists of the six biotite and white mica samples from the lower HNC and uppermost RNC units within the NSZ. These micas range in age from 397.8 ± 1.0 to 387.1 ± 0.8 Ma and define the top-WSW shear fabrics within the NSZ (Fig. 8a). The other age group consists of those from biotite in the four footwall samples with ages that range between 389.3 ± 0.8 and 378.3 ± 0.9 Ma. The rocks in the footwall lack a dominant top-WSW fabric and instead contain remnant top-ENE contractional fabrics, overprinted by a 'general shear' fabric best developed in the protomylonite sample H-2D, and related to doming during decompression of the footwall package (Osmundsen et al. 2003; Larsen et al. 2002). We thus distinguish *crystallization* ages, effectively 'dating' the genesis of the top-WSW shear fabric, in the case of the older group of 398-387 Ma micas in the NSZ, from *cooling* ages, 'dating' footwall unroofing/doming, in the case of the 389-378 Ma biotites.

This distinction of $^{40}Ar/^{39}Ar$ crystallization versus cooling ages is sustained for the NSZ micas for three related reasons: 1) reasonably coarse-grained white mica and biotite clearly define the top-WSW fabric in the NSZ; 2) the main NSZ fabric is interpreted to have been generated largely under lower amphibolite- to upper greenschist-facies metamorphic conditions (Osmundsen et al. 2003); 3) argon closure temperatures for biotite and white mica assumed in this study (ca. 300-400°C) broadly overlap with temperature conditions for lower amphibolite-facies metamorphism (Fig. 8b). In contrast, the biotites dated in the footwall cannot be linked to a single structural fabric, with exception of the protomylonite which has a fabric unrelated to that in the NSZ. In the Sjona window and Træna gneisses, the amphibolite-facies metamorphism related to contractional deformation was dated to 424-428 Ma, whilst the onset of decompressional melting related to doming was active by ca. 409 Ma and continued to at least 398 Ma (U-Pb data; Larsen et al. 2002) (Fig. 2). Unroofing clearly continued subsequent to this partial melting period with biotite ages from the footwall that indicate the majority of the Sjona window and RNC (below the NSZ) cooled below temperatures of ca. 300-350°C between 378 and 385 Ma (Fig. 8b). The 389 Ma age from one Sjona biotite sample implies a thermal gradient within the footwall more complex than the simple linear thermal profile depicted in Figure 8b. The protomylonite fabric at the margin of the Sjona window (378 Ma) is a late-stage product connected to unroofing-doming activity, perhaps related to local shear heating and later cooling, relative to other parts of the footwall.

The distinction we make between crystallization ages in the NSZ and younger, cooling ages in the footwall should not be divorced from the larger picture of progressive deformation and unroofing of the entire tectonostratigraphic package, including nappe, shear zone and footwall, in Devonian time. From at least 398 Ma, the NSZ was undergoing both top-WSW elongation and shortening (folding) perpendicular to the maximum elongation direction (Fig. 8b). The start of activity on the NSZ at 398 Ma overlaps in time with the decompression-related partial melting documented in the footwall at Træna (409-398 Ma; Larsen et al. 2002), so the shear activity in the middle-upper crust (NSZ) was not decoupled in time from unroofing at deeper levels. This accords well with the linked scenario of contractional strain within the lower crust and extensional tectonics operative in the middle-upper crust in an overall framework of Early-Middle Devonian top-W to -SW ductile extension, extension-normal shortening and sinistral strike-slip. Such a regime is proposed for mid- to north-central Norway during the waning phases of oblique continent-continent collision (Osmundsen et al. 2003; Braathen et al. 2002). In north-central Norway, the NSZ played a critical role in this deformation and unroofing process and if extended farther

north, as suggested by Osmundsen et al. (2003), the NSZ could also have acted as a major low-angle extensional shear zone that aided in Devonian unroofing in the Lofoten-Ofoten area (Fig. 1) (see also Olesen et al. 2002). The mica ages from this study allow us to bracket these activities in time, and to conclude that the major top-WSW shearing activity on the NSZ occurred largely between 398 and 387 Ma, with shear and extension waning by latest Middle Devonian time. Unroofing in the footwall had commenced already by 409-398 Ma (Larsen et al. 2002), but the footwall rocks did not pass through Ar-mica closure temperatures until 389-378 Ma. Unroofing, or 'doming', of the gneiss window was almost certainly promoted, and perhaps accelerated, by the earlier, NSZ-related extension in the overlying nappe pile.

The K-feldspar data from the Sjona window retain: 1) relicts of the Late Devonian doming, unroofing and cooling signature also recorded by biotites from the same rocks; 2) an Early Carboniferous signature, dominating the majority of the gas release. On the basis of the relict, low-gas volume, Late Devonian ages, we conclude that some highly retentive portion(s) of the feldspar structures closed to argon loss at temperatures probably only slightly below those of biotite during this time interval. However, the predominant, Early Carboniferous age signatures in the feldspars (varying between ca. 335 and 346 Ma), indicate that part of the feldspar system remained open (or was re-opened) to argon loss at least through Early Carboniferous time. Preliminary MDD modeling of the feldspars indicates that the age profiles of the feldspars are satisfactorily reproduced with a thermal history that includes rapid cooling (5-15°C/m.y.) in the period ca. 350-330 Ma. The cooling history between ca. 380-350 Ma is less well-constrained by the model, but is reproduced satisfactorily with slow cooling (<2°C/m.y.) for the period. We tentatively link the rapid, Early Carboniferous cooling to rapid unroofing promoted by activity on steep, ductile-to-brittle, low-greenschist facies shear zones that overrode lower-angle, medium-grade extensional shear zones like the NSZ (Fig. 8b) (Osmundsen et al. 2003; Braathen et al. 2002). Expressions of these faults include the western margins of the Rombak, Børgefjell and Nasafjäll windows, and may include the Kollstraumen detachment, which cross-cuts the NSZ in the south (Fig. 1). Border faults of this nature may also be present in the nearshore regions of north-central Norway, notably along the eastern margins of the Trøndelag Platform (Fig. 1; Osmundsen et al. 2002). Precise dating of these steeper and younger faults is necessary to test their correspondence in time to one another and to the Early Carboniferous unroofing event. We note that these younger faults are not folded, thus they must all post-date activity on folded shear-zones like the NSZ.

In western and southwestern Norway, rapid, Early Carboniferous cooling related to unroofing has also been proposed on the basis of K-feldspar $^{40}Ar/^{39}Ar$ ages and MDD modeling (Dunlap & Fossen 1998; Eide et al. 1999). The Early Carboniferous K-feldspar signatures from this study complement the results from southern and western Norway and we propose that Early Carboniferous rapid cooling and unroofing is a feature common throughout hinterland areas of the Scandinavian Caledonides. Such a result is critical for these areas where controls on Carboniferous and younger tectonic events are more difficult to obtain due to erosion of sedimentary rocks younger than Devonian in age. These Early Carboniferous feldspar signatures facilitate links to other areas in the North Atlantic perimeter (including the UK, Svalbard and East Greenland) and Siberia, where significant unconformities, igneous activity and inversion of basins of latest Devonian-Early Carboniferous ages are well documented (Vogt 1929; Harland et al. 1984; Torsvik et al. 1986; Nikishin et al. 1996; Bergh et al. 1997). While several 'far-field' explanations for this regional phenomenon have been proposed, many interpretations converge on the relationship between latest Devonian-Early Carboniferous 'events' and continuation/enhancement of the transcurrent motion along the Laurentia-Baltica suture in the waning phases of oblique Caledonian collision (Harland et al. 1984; Torsvik et al. 1996; Osmundsen et al. 1998; Krabbendam & Dewey 1998).

Conclusions

$^{40}Ar/^{39}Ar$ ages from micas and K-feldspars sampled in a profile through the low-angle, ductile Nesna Shear Zone and the underlying Sjona window yield evidence for linked, but kinematically distinct latest Early-Late Devonian top-WSW ductile extension and footwall unroofing, followed by another episode of rapid unroofing in Early Carboniferous time. The activity on the NSZ is constrained to have started at least by 398 Ma (biotite), and was waning by 387 Ma (biotite). Unroofing in the accompanying footwall biotites through closure temperatures similar to those of the NSZ micas took place between 389 and 378 Ma. Shearing and unroofing of latest Early-Late Devonian age took place in an evolving strain field for the mid- and north-central Scandinavian Caledonides where orogen-parallel extensional shearing at middle-upper crustal levels was accompanied by contraction normal to the extension direction in middle-lower crustal levels. This strain field, which also incorporated a component of sinistral shear, was effected during the last gasps of the oblique convergence characterizing Baltica-Laurentia collision. The Early Carboniferous unroofing documented by the feldspars in this study may be tentatively linked to activity on steeper, ductile-to-brittle extensional faults that reworked and cut the earlier, low-angle ductile shear and detachment zones, but which we propose were

active as part of a more regional phase of latest Devonian-Early Carboniferous tectonics that affected the entire North Atlantic perimeter.

The results from this study provide the first constraints for the time of initiation and duration of activity on a prominent, top-WSW crustal-scale detachment, the Nesna Shear Zone, which is traceable offshore (Olesen et al. 2002). Quantitative information on the ages and kinematics of an evolving, Late Paleozoic shear zone with both on- and offshore expression allows us to advance our understanding of the evolution of basement substrate of the rifted Norway margin.

Acknowledgements. - The authors thank the following BAT project sponsors for their strong support during the past five years: Norsk Agip, BP, ChevronTexaco, ConocoPhillips, ExxonMobil, Norsk Hydro, Norske Shell and Statoil. Research affiliations and exchanges with The Norwegian Petroleum Directorate and the University of Oslo have also been of benefit to the project. Thanks also to careful and constructive reviews by Brad Hacker and Øystein Larsen. The manuscript also benefitted from discussions with Tim Redfield and Trond Torsvik, who also read early versions of the manuscript.

References

Andersen, T.B., Berry, H.N., Lux, D.R. & Andresen, A. 1998: The tectonic significance of pre-Scandian $^{40}Ar/^{39}Ar$ phengite cooling ages in the Caledonides of western Norway. *Journal of the Geological Society, London 155*, 297-309.

Anderson, M.W., Barker, A.J., Bennett, D.G. & Dallmeyer, R.D. 1992: A tectonic model for Scandian terrane accretion. *Journal of the Geological Society, London 149*, 727-741.

Bergh, S.G.; Braathen, A. & Andresen, A. 1997: Interaction of basement-involved and thin-skinned tectonism in the Teritary fold-thrust belt of central Spitsbergen, Svalbard. *AAPG Bulletin 81*, 637-661.

Boundy, T.M., Essene, E.J., Hall, C.M., Austrheim, H. & Halliday, A.N. 1996: Rapid exhumation of lower crust during continent-continent collision and late extension: Evidence from $^{40}Ar/^{39}Ar$ incremental heating of hornblendes and muscovites, Caledonian orogen, western Norway. *Geological Society of America Bulletin 108*, 1425-1437.

Braathen, A., Nordgulen, Ø., Osmundsen, P.T., Andersen, T.B., Solli, A. & Roberts, D. 2000: Devonian, orogen-parallel, opposed extension in the Central Norwegian Caledonides. *Geology 28*, 615-618.

Braathen, A., Osmundsen, P. T., Nordgulen, Ø., Roberts, D. & Meyer, G. B. 2002: Orogen-parallel extension of the Caledonides in northern Central Norway: an overview. *Norwegian Journal of Geology 82(4)*, 225-241.

Chauvet, A. & Dallmeyer, R.D. 1992: $^{40}Ar/^{39}Ar$ mineral dates related to Devonian extension in the southwestern Scandinavian Caledonides. *Tectonophysics 210*, 155-177.

Coates, B.H., Zeltner, D.L., Carter, B.T., Steltenpohl, M.G., Andresen, A. & Kunk, M.J. 1999: $^{40}Ar/^{39}Ar$ and structural investigations of extensional development of the North-Central Norwegian margin. *Abstracts with programs, Geological Society of America 31 (7)*, 118.

Cocks, L.R.M. & Torsvik, T.H. 2002: Earth geography from 500 to 400 million years ago: a faunal and palaeomagnetic review. *Journal of the Geological Society, London 159*, 631-644.

Coker, J.E., Steltenpohl, M.G., Andresen, A. & Kunk, M.J. 1995: An $^{40}Ar/^{39}Ar$ thermochronology of the Ofoten-Troms region: Implications for terrane amalgamation and extensional collapse of the northern Scandinavian Caledonides. *Tectonics 14*, 435-447.

Corfu, F. & Emmett, T. 1992: U-Pb age of the Leirungsmyran gabbroic complex, Jotun Nappe, southern Norway. *Norsk Geologisk Tidsskrift 72*, 369-374.

Corfu, F. & Evins, P.M. 2002: Late Palaeoproterozoic monazite and titanite U-Pb ages in the Archean Suomujärvi Complex, N-Finland. *Precambrian Research 116*, 171-181.

Dallmeyer, R.D. 1988: Polyphase tectonothermal evolution of the Scandinavian Caledonides. *In* Harris, A.L. & Fettes, D.J. (eds.) *The Caledonian-Appalachian Orogen*, 365-379. Geological Society Special Publication 38.

Dallmeyer, R.D. 1990: $^{40}Ar/^{39}Ar$ mineral age record of a polyorogenic evolution with the Seve and Köli nappes, Trøndelag, Norway. *Tectonophysics 179*, 199-226.

Dallmeyer, R.D. & Andresen, A. 1992: Polyphase tectonothermal evolution of exotic Caledonian nappes in Troms, Norway: Evidence from $^{40}Ar/^{39}Ar$ mineral ages. *Lithos 29*, 19-42.

Dallmeyer, R.D., Gee, D.G. & Beckholmen, M. 1985: $^{40}Ar/^{39}Ar$ mineral age record of early Caledonian tectonothermal activity in the Baltoscandian miogeocline, central Scandinavia. *American Journal of Science 285*, 532-568.

Dalrymple, G.B., Alexander, E.C., Lanphere, M.A. & Kraker, G.P. 1981: Irradiation of samples for $^{40}Ar/^{39}Ar$ dating using the Geological Survey TRIGA reactor. *Geological Survey Professional Paper 1176*, 1-55.

Duffield,W.A. & Dalrymple, G.B. 1990: The Taylor Creek Rhyolite of New Mexico; a rapidly emplaced field of lava domes and flows. *Bulletin of Volcanology 52*, 475-487.

Dunlap, W.J. & Fossen, H. 1998: Early Paleozoic orogenic collapse, tectonic stability, and late Paleozoic continental rifting revealed through thermochronology of K-feldspars, southern Norway. *Tectonics 17*, 604-520.

Dunning, G.R. & Pedersen, R.-B. 1988: U/Pb dating of ophiolites and arc-related plutons of the Norwegian Caledonides: implications for the development of the Iapetus Ocean. *Contributions to Mineralogy and Petrology 98*, 13-23.

Eide, E.A. & Lardeaux, J.-M. 2002: An Ordovician blueschist in metaophiolite from the central Norwegian Caledonides—discovery and consequences. *Lithos 60*, 1-19.

Eide, E.A., Torsvik, T.H. & Andersen, T.B. 1997: Absolute dating of brittle fault movements: Late Permian and late Jurassic extensional fault breccias in western Norway. *Terra Nova 9*, 135-139.

Eide, E.A., Torsvik, T.H., Andersen, T.B. & Arnaud, N.O. 1999: Early Carboniferous unroofing in western Norway: A tale of alkali feldspar thermochronology. *Journal of Geology 107*, 353-374.

Fossen, H. & Dallmeyer, R.D. 1998: $^{40}Ar/^{39}Ar$ muscovite dates from the nappe region of southwestern Norway: dating extensional deformation in the Scandinavian Caledonides. *Tectonophysics 285*, 119-133.

Fossen, H. & Dunlap, W.J. 1998: Timing and kinematics of Caledonian thrusting and extensional collapse, southern Norway: evidence from $^{40}Ar/^{39}Ar$ thermochronology. *Journal of Structural Geology 20*, 765-781.

Grønlie, A. & Torsvik, T.H. 1989: On the origin and age of hydrothermal thorium-enriched carbonate veins and breccias in the Møre-Trøndelag Fault Zone, central Norway. *Norsk Geologisk Tidsskrift 69*, 1-19.

Grønlie, A., Harder, V. & Roberts, D. 1990: Preliminary fission-track ages of fluorite mineralisation along fracture zones, inner Trondheimsfjord, Central norway. *Norsk Geologisk Tidsskrift 70*, 173-178.

Gustavson, M. & Gjelle, S.T. 1991: Mo i Rana. Berggrunnsgeologisk kart, 1:250 000. *Norges geologiske undersøkelse.*

Hames, W.E. & Andresen, A. 1996: Timing of Paleozoic orogeny and

extension in the continental shelf of north-central Norway as indicated by laser $^{40}Ar/^{39}Ar$ muscovite dating. *Geology 24*, 1005-1008.

Harland, W.B., Gaskell, B.A., Heafford, A.P., Lind, E.K. & Perkins, P.J. 1984: Outline of Arctic post-Silurian continental displacements. In Spencer, A. M., et al., (eds.) *Petroleum Geology of the North European Margin*, 137-148. Graham & Trotman, London.

Harrison, T.M. 1981: Diffusion of ^{40}Ar in hornblende. *Contributions to Mineralogy and Petrology 78*, 324-331.

Hendricks, B.W.H., Huigen, Y.D., Murrell, G.R., Andriessen, P.A.M. & Cloetingh, S.A.P.L. 2002: Longterm morphotectonic evolution in Scandinavia; quantification and timing of vertical motions with constraints from fission track thermochronology (abstract). European Union of Geosciences 10, *Journal of Conference Abstract 4*, 452.

Jaffey, A.H., Flynn, K.F., Glendenin, L.E., Bentley, W.C. & Essling, A.M. 1971: Precision measurement of half-lives and specific activities of ^{235}U and ^{238}U. *Physical Reviews, Section C Nuclear Physics 4*, 1889-1906.

Klein, A.C., Steltenpohl, M.G., Hames, W.E. & Andresen, A. 1999: Ductile and brittle extension in the southern Lofoten archipelago, north Norway: Implications for differences in tectonic style along an ancient collisional margin. *American Journal of Science 299*, 69-89.

Krabbendam, M. & Dewey, J.F. 1998: Exhumation of UHP rocks by transtension in the Western Gneiss region, Scandinavian Caledonides. *In* Holdsworth, R E., Strachan, R.A. & Dewey, J.F. (eds.) *Continental transpressional and transtensional tectonics*, 159-181. The Geological Society, London, Special Publications *135*.

Krogh, T.E. 1982: Improved accuracy of U-Pb zircon ages by the creation of more concordant systems using an air abrasion technique. *Geochimica et Cosmochimica Acta 46*, 637-649.

Larsen, Ø., Skår, Ø. & Pedersen, R.-B. 2002: U-Pb zircon and titanite geochronological constraints on the late/post-Caledonian basement evolution of the Scandinavian Caledonides in north-central Norway. *Norwegian Journal of Geology 82(2)*, 1-13.

Ludwig, K.R. 1999: Isoplot/Ex version 2.03. A geochronological toolkit for Microsoft Excel. *Berkeley Geochronology Center Special Publication 1*, 43pp.

McDougall, I. & Harrison, T.M. 1999: *Geochronology and Thermochronology by the $^{40}Ar/^{39}Ar$ method*. Oxford Monographs on Geology and Geophysics no. 9, Second Edition. Oxford University Press, New York, 269pp.

Nikishin, A.M., Ziegler, P.A., Stephenson, R.A., Cloetingh, S.A.P.L., Furne, A.V., Fokin, P.A., Ershov, A.V., Bolotov, S.N., Korotaev, M.V., Alekseev, A.S., Gorbachev, V.I., Shipolov, E.V., Lankreijer, A., Bembinova, E.Yu, & Shalimov, I.V. 1996: Late Precambrian to Triassic history of the East European Craton: dynamics of sedimentary basin evolution. *Tectonophysics 268*, 23-63.

Nordgulen, Ø., Bickford, M.E., Nissen, A.L. & Wortman, G.L. 1993: U-Pb zircon ages from the Bindal Batholith, and the tectonic history of the Helgeland Nappe Complex, Scandinavian Caledonides. *Journal of the Geological Society London 150*, 771-783.

Northrup, C.J. 1997: Timing structural assembly, metamorphism, and cooling of Caledonian nappes in the Ofoten-Efjorden area, north Norway: Tectonic insights from U-Pb and $^{40}Ar/^{39}Ar$ geochronology. *Journal of Geology 105*, 565-582.

Olesen, O., Lundin, E., Nordgulen, Ø., Osmundsen, P.T., Skilbrei, J.R., Smethurst, M.A., Solli, A., Bugge, T. & Fichler, C. 2002: Bridging the gap between the onshore and offshore geology in Nordland, northern Norway. *Norwegian Journal of Geology 82(4)*, 243-262.

Osmundsen, P.T., Andersen, T.B., Markussen, S. & Svendby, A.K. 1998: Tectonics and sedimentation in the hanging wall of a regional extensional detachment: the Devonian Kvamshesten basin, W. Norway. *Basin Research 10*, 213-234.

Osmundsen, P.T., Braathen, A., Nordgulen, Ø., Roberts, D., Meyer, G.B. & Eide, E. 2003. The Devonian Nesna shear zone and adjacent gneiss-cored culminations, North-Central Norwegian Caledonides. *Journal of the Geological Society, London 160*, 1-14.

Osmundsen, P.T., Sommaruga, A., Skilbrei, J.R. & Olesen, O. 2002. Deep structure of the Norwegian Sea area, North Atlantic margin. *Norwegian Journal of Geology 82(4)*, 205-224.

Redfield, T.F., Torsvik, T.H., Andriessen, P.A.M. & Gabrielsen, R.H. accepted: Mesozoic and Cenozoic tectonics of the Møre Trøndelag Fault Complex, central Norway: constraints from new apatite fission track data. *Physics and Chemistry of the Earth* (in press).

Rex, D.C. & Guise, P.G. 1995: Evaluation of argon standards with special emphasis on time scale measurements. *In* Odin, G.S. (ed.) *Phanerozoic Time Scale*, 21-23. Bulletin Lias. Information, IUGS Subcommission on Geochronology *13*.

Roberts, D. 1998: High-strain zones from meso- to macro-scale at different structural levels, Central Norwegian Caledonides. *Journal of Structural Geology 20*, 111-119.

Roberts, D. & Gee, D.G. 1985: An introduction to the structure of the Scandinavian Caledonides. *In* Gee, D.G. & Sturt, B.A. (eds.) *The Caledonide orogen – Scandinavia and related areas*, 55-68. John Wiley & Sons, Chichester.

Roberts, D., Sturt, B.A. & Furnes, H. 1985: Volcanite assemblages and environments in the central Norwegian Caledonides and the sequential development history of the mountain belt. *In* Gee, D.G. & Sturt, B.A. (eds.) *The Caledonide orogen – Scandinavia and related areas*, 919- 930. John Wiley & Sons, Chichester.

Rykkelid, E. & Andresen, A. 1994: Late Caledonian extension in the Ofoten area, northern Norway. *Tectonophysics 231*, 157-169.

Schärer, U. 1980: U-Pb and Rb-Sr dating of a polymetamorphic nappe terrain: The Caledonian Jotun Nappe, southern Norway. *Earth and Planetary Science Letters 49*, 205-218.

Solli, A. 1995: Digitalt berggrunnskart over Nord-Trøndelag og Fosen. *Norges geologiske undersøkelse.*

Solli, A. 1999: Berggrunnskart over Nordland. *Norges geologiske undersøkelse.*

Solli, A., Robinson, P. & Tucker, R.D. 1997: Proterozoic basement and Scandian geology of the Outer Trondheimsfjord region. *Norges geologiske undersøkelse report 97.133*, 21pp.

Stacey, J.S. & Kramers, J.D. 1975: Approximation of terrestrial lead isotope evolution by a two-stage model. *Earth and Planetary Science Letters 34*, 207-226.

Stephens, M. & Gee, D.G. 1985: A tectonic model for the evolution of the eugeoclinal terranes in the central Scandinavian Caledonides. In Gee, D.G. & Sturt, B.A. (eds.) *The Caledonide orogen – Scandinavia and related areas*, 953- 978. John Wiley & Sons, Chichester.

Stephens, M., Gustavson, M., Ramberg, I.B: & Zachrisson, E. 1985: The Caledonides of central-north Scandinavia – a tectonostratigraphic overview. *In* Gee, D.G. & Sturt, B.A. (eds.) *The Caledonide orogen – Scandinavia and related areas*, 135- 162. John Wiley & Sons, Chichester.

Torsvik, T.H. 1998: Palaeozoic palaeogeography: A North Atlantic viewpoint. *GFF 120*, 109-118.

Torsvik, T.H., Smethurst, M.A., Meert, J.G., Van der Voo, R., McKerrow, W. S., Brasier, M. D., Sturt, B. A. & Walderhaug, H. J. 1996: Continental break-up and collision in the Neoproterozoic and Palaeozoic—a tale of Baltica and Laurentia. *Earth Science Reviews 40*, 229-258.

Torsvik, T.H., Sturt, B.A., Ramsay, D.M., Kisch, H.J. & Bering, D. 1986: The tectonic implications of Solundian (Upper Devonian) magnetization of the Devonian rocks of Kvamshesten, western Norway. *Earth and Planetary Science Letters 80*, 337-347.

Tucker, R.D., Bradley, D.C., Ver Straeten, C.A., Harris, A.G., Ebert, J.R. & McCutcheon, S.R. 1998: New U-Pb zircon ages and the duration and division of Devonian time. *Earth and Planetary Science Letters 158*, 175-186.

Tucker, R.D., Krogh, T.E. & Råheim, A. 1991: Proterozoic evolution and age-province boundaries in the central part of the Western Gneiss Region, Norway: Results of U-Pb dating and accessory

minerals from Trondheimsfjord to Geiranger. *Geological Association of Canada, Special Paper 38*, 149-173.

Tucker, R.D., Råheim, A., Krogh, T.E. & Corfu, F. 1987: Uranium-lead zircon and titanite ages from the northern portion of the Western Gneiss Region, south-central Norway. *Earth and Planetary Science Letters 81*, 203-211.

Turner, G., Huneke, J.C., Podosek, F.A. & Wasserburg, G.J. 1971: ^{40}Ar-^{39}Ar ages and cosmic ray exposure ages of Apollo 14 samples. *Earth and Planetary Science Letters 12*, 19-35.

Vogt, T. 1929: Den norske fjellkjedes revolusjons-historie. *Norsk Geologisk Tidsskrift 10*, 97-115.

Yoshinobu, A.S., Barnes, C.G., Nordgulen, Ø., Prestvik, T., Fanning, M. & Pedersen, R.-B. 2002: Ordovician magmatism, deformation, and exhumation in the Caledonides of central Norway: An orphan of the Taconic orogeny? *Geology 30*, 883–886.

Appendix 1. Analytical procedures, Geological Survey of Norway $^{40}Ar/^{39}Ar$ Geochronology Laboratory; analytical procedures, Geological Museum, TIMS laboratory.

Mineral separates were obtained using standard techniques: the rocks were crushed, washed and sieved to fraction size 250-350 mm (biotite and K-feldspars) and 350-500 mm (white mica). Magnetic separation and heavy liquids were used to obtain pure fractions of K-feldspars. Before packing in Al-foil, mineral separates were hand-picked under binocular microscope to exclude grains with visible inclusions and/or surface alteration; hand-picked material was subsequently rinsed in alternating acetone and distilled water. Sample packets were stacked and loaded in a sealed Al-capsule with Cd-shielding for irradiaton in the 5C site at the McMaster Nuclear Reactor facility, Hamilton, Canada. The samples at McMaster were irradiated for 25 hours (50 MWH) with nominal neutron flux of 4 x 10e13 n/cm^2/s; nominal temperature in the irradiation site is <50°C (M. Butler, pers. comm.). Production of isotopes from Ca and K were determined by irradiation of CaF and K_2SO_4 salts; values of 36/37Ca = 0.00035, 39/37Ca = 0.0011, and 40/39K = 0.022 were used. Neutron fluence monitors included Taylor Creek Rhyolite sanidine, Tinto biotite and Hb3gr hornblende with ages of 27.92 Ma (TCR; Duffield and Dalrymple, 1990), 410.3 Ma (Tinto; Rex and Guise, 1995) and 1072 ± 11 Ma (Hb3gr; Turner et al., 1971). Uncertainty in J-values for monitors in both irradiations ranged from 0.1 to 0.8 % without including error in monitor age; we incorporated a conservative 1% error in J-value for all unknowns.

Samples were analyzed at the $^{40}Ar/^{39}Ar$ Geochronology Laboratory at the Norwegian Geological Survey. Gas from irradiated samples was released in a step-wise fashion from a resistance furnace (built by Heine Associates with Eurotherm controller). Automated furnace temperature calibration was obtained by melting experiments (pure metals) coupled with measurements using an optical pyrometer. Uncertainties on individual temperature steps in the furnace are conservatively ±15°C.

Gas released from a sample at a single temperature step was cleaned in the extraction line for 11 minutes using two pairs of SAES AP-10 getters, mounted in isolated sections of the line, each maintained with their own vacuum pumps. On each of the getter pairs, one getter is maintained at room temperature while the other is maintained at 400°C. The purified gas was then analyzed on a MAP 215-50 mass spectrometer. Pneumatic valves on on both the extraction line and mass spectrometer are automated using LabView software (code written by M.O. McWilliams). Dynamic blank measurements on mass 40 indicate a stable background (2.19 x 10^{-14} ccSTP), barely above instrument background levels (between-mass signal levels).

Data for blanks, monitors and unknowns were collected on a Johnson electron multiplier with gain setting at 1, while the magnet was automatically scanned over masses 35 through 41 in a cycled, 'peak-hop' mode. Masses 37 through 40 were each measured in eight cycles with 10 counts per mass per cycle with exception of mass 36 which was measured with 20 counts per cycle. Background levels (blanks) for the furnace were measured at 100 to 200°C temperature increments prior to each sample analysis. Blanks were maintained at levels of 6-9 x 10^{-12} ccSTP for mass 40 and 7-9 x 10^{-14} ccSTP for mass 36 at temperatures of 500 through 1000°C; blanks increased to 1-9 x 10^{-11} ccSTP for mass 40 and 1-3 x 10^{-13} ccSTP for mass 36 at high temperatures (1200-1400°C). At experimental temperatures between 600 and 1000°C, furnace blanks for mass 40 were usually <1% of the sample signal size. Background levels of masses 37 and 39 did not change signficantly from dynamic blank levels at any temperature (2.1 x 10^{-13} ccSTP for mass 37; <3.3 x 10^{-14} ccSTP for mass 39). Background levels for mass 38 were at dynamic blank levels 1 x 10^{-13} ccSTP at high temperatures and <9 x 10^{-14} ccSTP at temperatures < 1000°C.

Data from unknowns were corrected for blanks prior to being reduced with the IAAA (Interactive Ar-Ar Analysis) software package (Visual Basic programming for PC Windows) written by T.H. Torsvik and N.O. Arnaud based on equations in Dalrymple et al. (1981) and McDougall and Harrison (1999). Data reduction in IAAA incorporates corrections for interfering isotopes, mass discrimination, error in blanks and decay of ^{37}Ar.

The U-Pb procedure was carried out by isotope dilution using a $^{205}Pb/^{235}U$ spike. Following mineral separation, zircon and titanite were picked under a binocular microscope, abraded (Krogh 1982), and dissolved at 185°C in teflon bombs (zircon) or on a hotplate in Savillex vials (titanite). U and Pb were separated from the solution using anion exchange resin with HCl for zircon and a combination of Hbr, HCl and HNO_3 for titanite. Details of the measurement procedure are given in Corfu and Evins (2002). Blank correction was 2 pg Pb and 0.1 pg U for zircon, and 10 pg Pb and 0.3 pg U for titanite, and initial Pb was corrected using Pb compositions calculated with the Stacey and Kramers (1975) model. The results were plotted and regressed using the software of Ludwig (1999). The decay constants are those of Jaffey et al. (1971). Uncertainties in the isotopic ratios and the ages are given and plotted at 2 sigma.

Appendix 2. Complete $^{40}Ar/^{39}Ar$ data tables from the Nesna Shear Zone-footwall profile.

Temp (C)	$^{40}Ar/^{39}Ar$	$^{38}Ar/^{39}Ar$	$^{37}Ar/^{39}Ar$	$^{36}Ar/^{39}Ar$	^{39}Ar	$F^{39}Ar$[1]	%40*[2]	$^{40}Ar^*/^{39}Ar_K$	Age (Ma)	±1σ
	H-2A biotite		**J=.0059390**							
500	42.349	0.001	0.052	36.260	9.873	1.92	74.7	31.62	310.63	1.38
550	44.221	0.001	0.007	18.890	15.935	5.01	87.3	38.62	372.72	2.01
600	42.998	0.001	0.016	16.697	20.782	9.04	88.5	38.04	367.72	1.29
640	58.060	0.000	0.007	61.864	28.078	14.48	68.5	39.76	382.64	0.94
675	41.058	0.000	0.003	4.415	35.559	21.38	96.8	39.73	382.41	0.72
700	40.813	0.001	0.000	3.316	33.781	27.94	97.5	39.81	383.10	0.64
725	41.328	0.001	0.000	5.672	25.562	32.89	95.9	39.63	381.53	1.29
750	44.432	0.002	0.000	15.354	18.367	36.46	89.7	39.87	383.63	0.51
785	44.976	0.001	0.000	15.096	14.176	39.21	90.0	40.49	389.00	1.04
820	46.295	0.000	0.033	19.790	11.875	41.51	87.3	40.43	388.46	2.20
860	43.455	0.000	0.013	11.783	18.586	45.12	91.9	39.95	384.33	0.64
900	41.752	0.001	0.000	4.793	38.183	52.52	96.6	40.31	387.45	0.71
950	40.367	0.001	0.001	2.947	89.915	69.97	97.8	39.47	380.17	0.40
1000	39.955	0.001	0.000	2.258	94.324	88.26	98.3	39.27	378.36	0.21
1050	39.902	0.001	0.002	2.710	48.339	97.64	97.9	39.08	376.74	0.39
1100	40.661	0.002	0.000	4.689	12.155	100	96.5	39.25	378.25	0.96
	H-2A K-feldspar		**J=.0059380**							
500	79.823	0.000	0.423	9.768	10.647	1.92	96.5	76.99	679.62	1.88
600	27.531	0.001	0.095	5.448	33.771	8.01	94.1	25.91	258.33	0.54
700	35.295	0.001	0.042	26.551	80.373	22.51	77.7	27.43	272.4	0.43
800	32.195	0.001	0.050	1.847	59.544	33.26	98.3	31.63	310.72	0.54
840	33.833	0.000	0.040	3.241	24.374	37.65	97.1	32.86	321.74	0.73
890	36.979	0.001	0.041	1.851	90.208	53.93	98.5	36.42	353.36	0.60
940	35.419	0.000	0.040	1.242	82.157	68.75	98.9	35.04	341.16	0.42
980	34.574	0.001	0.034	0.600	59.971	79.57	99.4	34.38	335.32	0.35
1020	34.972	0.002	0.036	0.698	27.213	84.48	99.4	34.75	338.61	0.58
1070	35.831	0.002	0.000	2.244	12.476	86.73	98.1	35.15	342.13	1.14
1130	38.744	0.001	0.000	0.957	12.539	88.99	99.2	38.44	371.11	0.95
1190	37.962	0.001	0.000	2.140	16.824	92.03	98.3	37.31	361.21	0.63
1250	36.873	0.000	0.000	1.922	21.856	95.97	98.4	36.28	352.19	1.01
1320	37.897	0.000	0.000	2.098	20.021	99.58	98.3	37.26	360.74	0.93
1400	51.17	0.004	0.000	28.812	2.325	100	83.3	42.63	407.34	5.64
	H-2B biotite		**J=.0059370**							
500	51.135	0.018	0.710	44.100	40.340	2.59	74.7	38.18	368.83	0.80
550	43.391	0.011	0.127	11.875	72.171	7.23	91.9	39.88	383.57	0.68
590	42.045	0.011	0.258	7.202	119.687	14.91	95.0	39.93	384.03	0.45
620	43.703	0.012	0.029	11.171	160.420	25.22	92.4	40.38	387.94	0.40
640	41.869	0.010	0.129	5.120	159.753	35.48	96.4	40.35	387.67	0.55
660	41.780	0.011	0.000	3.679	143.798	44.71	97.3	40.67	390.42	0.40
680	41.256	0.009	0.087	2.176	92.390	50.65	98.4	40.60	389.83	0.56
700	41.206	0.011	0.118	2.024	58.300	54.39	98.5	40.60	389.83	0.70
730	41.283	0.012	0.000	2.203	48.562	57.51	98.4	40.61	389.89	0.70
760	41.461	0.009	0.346	3.289	76.314	62.41	97.7	40.52	389.10	0.53
800	40.948	0.011	0.000	2.141	171.408	73.42	98.4	40.29	387.15	0.37
830	41.344	0.009	0.006	2.564	180.985	85.05	98.1	40.57	389.51	0.29
860	41.786	0.010	0.519	5.477	79.795	90.17	96.3	40.22	386.54	0.53
890	42.177	0.011	0.000	4.341	78.092	95.19	96.9	40.87	392.15	0.61
930	42.203	0.011	0.000	5.606	66.891	99.48	96.0	40.52	389.15	0.46
970	49.970	0.018	0.000	34.353	8.063	100	79.6	39.80	382.86	2.92

Temp (C)	$^{40}Ar/^{39}Ar$	$^{38}Ar/^{39}Ar$	$^{37}Ar/^{39}Ar$	$^{36}Ar/^{39}Ar$	^{39}Ar	$F^{39}Ar^{1}$	%40*[2]	$^{40}Ar^{*}/^{39}Ar_{K}$	Age (Ma)	±1σ
H-2B K-feldspar			**J=.0059350**							
400	62.911	0.001	0.385	5.367	1.491	0.13	97.5	61.37	560.62	3.63
400	26.963	0.006	0.000	2.506	1.995	0.31	97.2	26.20	260.89	3.46
450	28.689	0.007	0.000	1.817	4.404	0.71	98.1	28.13	278.70	1.80
450	25.461	0.004	1.259	1.947	4.110	1.08	98.3	25.03	250.00	1.96
500	25.452	0.007	0.000	0.013	7.864	1.78	99.9	25.43	253.70	0.97
550	27.496	0.008	0.462	1.421	16.187	3.23	98.6	27.12	269.35	1.30
550	26.216	0.010	0.000	1.540	16.238	4.69	98.2	25.74	256.60	0.98
600	28.645	0.005	0.000	2.346	28.564	7.25	97.5	27.93	276.85	0.62
600	27.489	0.008	0.000	2.228	25.582	9.55	97.5	26.81	266.52	1.06
650	28.523	0.006	0.128	0.608	36.185	12.79	99.4	28.34	280.61	0.89
700	31.132	0.007	0.136	0.725	55.207	17.74	99.3	30.91	304.07	0.87
700	34.412	0.006	0.000	0.676	60.619	23.18	99.4	34.19	333.49	1.67
750	31.780	0.010	0.000	1.098	26.408	25.55	98.9	31.43	308.77	2.41
800	32.247	0.006	0.061	0.760	28.930	28.14	99.3	32.01	313.95	0.82
800	32.441	0.006	0.191	1.026	21.442	30.06	99.1	32.14	315.16	1.02
800	33.392	0.006	0.059	0.705	19.868	31.84	99.3	33.17	324.38	1.01
800	34.497	0.007	0.000	1.322	31.008	34.63	98.8	34.08	332.54	1.00
750	35.955	0.009	5.928	0.405	2.470	34.85	102.0	36.67	355.39	5.01
800	34.489	0.006	3.473	1.647	6.073	35.39	99.9	34.47	335.99	1.67
850	34.713	0.004	1.797	2.090	14.352	36.68	98.9	34.33	334.70	0.75
950	33.458	0.005	0.000	1.114	54.743	41.59	99.0	33.11	323.81	0.52
1000	33.564	0.010	0.000	1.939	161.942	56.11	98.2	32.97	322.57	0.14
1040	35.056	0.006	0.036	0.216	258.942	79.33	99.8	34.98	340.47	1.19
1070	34.210	0.007	0.265	0.548	73.050	85.88	99.6	34.06	332.35	1.27
1140	34.344	0.008	0.000	0.668	35.922	89.10	99.4	34.12	332.90	0.84
1170	35.049	0.008	0.881	1.086	26.697	91.50	99.4	34.83	339.18	1.27
1220	36.163	0.007	0.278	0.710	25.370	93.77	99.5	35.97	349.28	1.46
1270	35.517	0.007	0.000	0.314	25.490	96.06	99.7	35.40	344.25	2.47
1350	38.510	0.006	0.282	0.615	43.932	100	99.6	38.35	370.13	0.90
H-2C K-feldspar			**J=.0059310**							
400	346.741	0.002	0.000	23.262	1.032	0.14	98.0	339.85	1992.43	7.95
450	55.132	0.000	0.000	0.052	1.929	0.40	99.9	55.09	510.37	0.84
450	26.554	0.000	0.000	0.051	1.946	0.67	99.9	26.52	263.65	0.76
500	40.354	0.000	0.163	1.099	4.549	1.29	99.2	40.03	384.53	2.14
500	25.416	0.001	0.000	0.666	4.504	1.90	99.1	25.20	251.41	2.10
550	32.818	0.003	0.000	0.332	9.034	3.13	99.6	32.70	319.95	1.26
550	27.012	0.005	0.000	0.011	9.251	4.39	99.9	26.99	268.00	0.33
600	29.450	0.005	0.000	1.773	16.361	6.61	98.1	28.90	285.61	0.83
600	27.103	0.005	0.000	1.092	16.487	8.86	98.7	26.76	265.89	0.75
650	33.330	0.006	0.000	18.779	20.235	11.61	83.3	27.76	275.11	1.63
650	28.399	0.005	0.206	0.692	21.663	14.56	99.3	28.20	279.16	0.58
700	30.796	0.003	0.000	0.720	27.773	18.34	99.2	30.56	300.69	0.44
700	35.291	0.005	0.000	0.442	33.970	22.96	99.6	35.14	341.70	0.30
750	37.416	0.007	0.146	1.282	35.892	27.85	99.0	37.04	358.43	1.65
750	38.347	0.004	0.000	1.115	20.634	30.65	99.1	38.00	366.84	1.03
800	38.768	0.007	1.219	0.969	15.480	32.76	99.7	38.64	372.44	4.24
800	36.387	0.004	0.000	1.549	11.622	34.34	98.7	35.91	348.50	1.12
800	36.361	0.002	1.300	1.718	11.058	35.85	99.1	36.02	349.47	1.35
750	40.104	0.005	0.000	0.073	1.379	36.03	99.9	40.06	384.79	3.32
800	38.255	0.005	0.000	2.116	3.308	36.48	98.3	37.61	363.44	3.50
880	37.180	0.003	0.000	2.878	11.815	38.09	97.7	36.31	352.03	1.33
920	34.513	0.007	0.787	2.311	21.200	40.98	98.3	33.92	330.86	0.77
950	35.278	0.002	0.000	0.815	25.775	44.48	99.3	35.01	340.61	0.88
980	33.360	0.004	0.152	0.632	30.048	48.57	99.4	33.17	324.20	1.37
1010	35.079	0.006	0.953	1.120	29.468	52.58	99.4	34.86	339.24	0.54
1040	35.447	0.006	0.720	1.072	24.251	55.88	99.3	35.21	342.34	0.35
1080	37.016	0.006	0.548	1.186	19.392	58.52	99.2	36.72	355.68	0.80
1120	39.413	0.001	1.070	1.619	14.206	60.46	99.1	39.07	376.19	0.79
1170	37.229	0.005	0.366	1.827	20.794	63.29	98.6	36.72	355.66	0.46
1230	35.430	0.006	0.137	1.535	144.640	82.97	98.7	34.97	340.24	0.96
1300	35.579	0.006	0.044	0.641	87.398	94.86	99.4	35.37	343.78	0.23
1350	37.660	0.006	0.000	0.847	37.760	100	99.3	37.39	361.51	1.23

Temp (C)	$^{40}Ar/^{39}Ar$	$^{38}Ar/^{39}Ar$	$^{37}Ar/^{39}Ar$	$^{36}Ar/^{39}Ar$	^{39}Ar	$F^{39}Ar^{1}$	%40*[2]	$^{40}Ar^{*}/^{39}Ar_{K}$	Age (Ma)	±1σ
	H-2D biotite		**J=.0059610**							
500	44.729	0.001	0.261	41.373	6.381	1.15	72.7	32.52	319.81	1.73
540	42.661	0.002	0.060	16.743	10.691	3.08	88.4	37.70	365.93	1.78
600	42.813	0.000	0.000	13.490	27.502	8.05	90.6	38.80	375.60	1.85
635	53.355	0.001	0.000	47.586	33.077	14.03	73.6	39.27	379.68	0.49
675	40.672	0.000	0.000	3.132	35.117	20.37	97.7	39.72	383.62	0.62
705	39.443	0.001	0.000	2.471	29.140	25.64	98.1	38.69	374.61	1.03
745	40.269	0.000	0.000	3.139	22.619	29.72	97.6	39.32	380.10	1.01
780	40.369	0.000	0.021	5.957	13.093	32.09	95.6	38.59	373.72	0.63
825	58.887	0.000	0.089	62.684	20.707	35.83	68.5	40.36	389.10	1.13
875	39.685	0.000	0.077	2.439	26.646	40.65	98.2	38.95	376.90	0.77
915	40.113	0.000	0.025	1.756	47.826	49.29	98.7	39.58	382.32	0.34
965	39.421	0.000	0.024	1.169	95.839	66.60	99.1	39.06	377.81	0.29
1000	39.365	0.001	0.000	1.005	95.543	83.86	99.2	39.05	377.71	0.29
1040	39.371	0.000	0.000	1.270	66.163	95.82	99.0	38.97	377.08	0.74
1075	39.470	0.001	0.000	1.900	23.158	100	98.5	38.89	376.32	0.40
	H-2D K-feldspar		**J=.0059710**							
400	42.045	0.008	0.000	14.225	2.671	0.36	90.0	37.82	367.53	2.21
450	23.029	0.006	0.000	4.354	5.512	1.09	94.3	21.72	220.11	1.11
450	22.240	0.007	2.339	5.777	4.155	1.64	93.6	20.81	211.38	1.73
500	22.778	0.006	0.000	1.976	9.108	2.85	97.3	22.17	224.43	0.71
500	22.539	0.007	0.000	1.679	8.934	4.04	97.7	22.02	222.98	0.87
550	24.140	0.008	0.253	1.840	17.931	6.43	97.8	23.61	238.02	0.47
550	24.333	0.007	0.585	2.760	17.752	8.79	96.9	23.57	237.69	1.32
600	26.111	0.005	0.000	2.894	29.719	12.74	96.6	25.23	253.33	0.75
600	24.727	0.009	0.000	2.234	27.309	16.38	97.2	24.04	242.16	0.61
650	30.429	0.006	0.266	14.044	29.337	20.28	86.4	26.29	263.22	0.94
650	27.606	0.001	0.356	1.340	32.838	24.65	98.7	27.24	271.99	1.08
700	28.665	0.007	0.000	0.776	41.225	30.13	99.1	28.41	282.87	1.05
700	29.487	0.005	0.314	0.611	39.300	35.36	99.5	29.33	291.27	1.17
750	30.586	0.005	0.000	0.130	15.380	37.41	99.8	30.53	302.23	0.66
750	30.752	0.006	0.000	0.737	13.560	39.21	99.2	30.51	302.10	0.58
800	32.403	0.005	0.160	1.214	16.477	41.41	98.9	32.04	316.02	0.54
800	45.123	0.006	0.000	25.719	13.142	43.15	83.1	37.50	364.72	1.37
800	35.898	0.004	0.000	3.193	35.390	47.86	97.3	34.93	341.96	1.02
800	34.296	0.005	0.174	0.856	60.734	55.94	99.3	34.05	334.04	0.79
750	34.221	0.005	0.105	0.160	6.264	56.78	99.8	34.17	335.12	0.77
800	33.975	0.005	0.096	0.799	13.775	58.61	99.3	33.73	331.21	1.18
840	34.571	0.004	0.000	0.555	19.822	61.25	99.5	34.38	337.07	0.56
880	34.046	0.005	0.000	0.398	30.167	65.26	99.6	33.91	332.79	0.31
920	33.141	0.006	0.000	0.569	38.690	70.41	99.4	32.95	324.20	1.04
960	34.337	0.005	0.050	0.710	39.447	75.66	99.3	34.11	334.64	0.79
990	34.780	0.006	0.625	0.805	28.574	79.46	99.5	34.61	339.07	1.07
1020	35.559	0.004	0.712	1.278	14.866	81.44	99.2	35.26	344.88	1.12
1050	36.864	0.006	0.337	0.848	11.790	83.00	99.4	36.64	357.12	0.95
1090	37.975	0.003	1.393	0.162	12.352	84.65	100.3	38.11	370.06	0.67
1130	38.461	0.005	2.091	0.961	14.568	86.59	100.0	38.46	373.15	0.79
1180	37.618	0.006	0.550	0.987	19.256	89.15	99.4	37.38	363.69	1.30
1230	37.173	0.007	0.353	0.568	28.160	92.89	99.6	37.03	360.61	1.89
1300	35.071	0.006	0.335	0.367	43.552	98.69	99.8	34.99	342.46	3.81
1350	39.193	0.008	0.606	1.116	9.854	100	99.3	38.93	377.26	1.45

Temp (C)	$^{40}Ar/^{39}Ar$	$^{38}Ar/^{39}Ar$	$^{37}Ar/^{39}Ar$	$^{36}Ar/^{39}Ar$	^{39}Ar	$F^{39}Ar^{1}$	%40*[2]	$^{40}Ar^{*}/^{39}Ar_{K}$	Age (Ma)	±1σ
	H-3 biotite		**J=.0059810**							
500	29.773	0.002	0.025	45.472	15.020	1.30	54.8	16.32	168.08	1.57
550	39.408	0.001	0.004	20.695	24.885	3.45	84.4	33.27	327.59	0.72
590	42.762	0.001	0.000	12.058	34.997	6.48	91.6	39.18	380.00	1.21
625	50.050	0.001	0.002	34.753	45.205	10.39	79.4	39.76	385.08	0.66
650	41.268	0.000	0.000	4.944	43.079	14.11	96.4	39.79	385.31	0.37
675	41.137	0.000	0.000	5.604	38.899	17.48	95.9	39.46	382.46	0.89
700	41.476	0.002	0.006	6.061	39.102	20.86	95.6	39.66	384.25	0.85
730	44.499	0.000	0.008	16.444	50.597	25.23	89.0	39.62	383.86	0.38
760	43.708	0.000	0.005	13.802	55.646	30.05	90.6	39.61	383.77	0.54
785	40.399	0.000	0.002	4.694	37.925	33.33	96.5	38.99	378.36	0.43
845	40.504	0.001	0.000	2.621	40.056	36.79	98.0	39.71	384.63	0.43
875	40.673	0.001	0.000	1.603	46.174	40.78	98.8	40.18	388.72	1.02
910	40.110	0.001	0.000	1.530	77.781	47.51	98.8	39.64	384.01	0.45
940	39.743	0.001	0.000	1.063	98.797	56.05	99.2	39.41	382.01	0.39
970	39.964	0.002	0.000	0.743	102.264	64.90	99.4	39.72	384.76	0.14
1000	39.639	0.000	0.000	1.053	111.059	74.50	99.2	39.31	381.12	0.16
1030	39.825	0.001	0.000	1.246	102.692	83.38	99.0	39.43	382.25	0.55
1060	39.725	0.000	0.002	1.465	98.300	91.89	98.9	39.27	380.81	0.33
1090	39.703	0.001	0.002	1.203	67.326	97.71	99.0	39.33	381.30	0.29
1120	39.954	0.001	0.004	2.076	26.496	100	98.4	39.32	381.24	0.58
	H-1A white mica		**J=.0059420**							
500	64.021	0.000	0.000	48.145	1.309	0.57	77.7	49.77	467.67	7.81
600	66.135	0.000	0.078	86.361	4.551	2.55	61.4	40.6	390.14	4.75
650	169.308	0.012	0.147	421.837	4.355	4.45	26.4	44.66	424.81	7.99
680	64.441	0.002	0.000	77.543	4.836	6.56	64.4	41.51	397.91	4.61
705	66.936	0.003	0.000	77.299	9.302	10.62	65.8	44.07	419.86	3.09
735	54.865	0.002	0.000	43.319	12.235	15.95	76.6	42.04	402.52	1.67
765	43.949	0.001	0.000	12.101	19.586	24.49	91.8	40.35	387.95	0.57
795	42.373	0.002	0.010	5.787	38.018	41.07	95.9	40.64	390.46	0.51
855	41.857	0.001	0.000	3.576	29.641	54.00	97.4	40.78	391.64	0.65
885	41.443	0.001	0.000	3.421	22.511	63.81	97.5	40.41	388.46	0.45
925	42.447	0.001	0.000	4.952	26.252	75.26	96.5	40.96	393.22	0.89
975	42.152	0.000	0.047	4.412	23.345	85.44	96.9	40.83	392.11	0.67
1025	42.343	0.000	0.011	3.623	33.395	100.00	97.4	41.25	395.72	0.52
	H-1B biotite		**J=.0059410**							
500	38.916	0.023	0.000	49.169	7.850	0.77	62.6	24.36	244.02	6.22
550	42.694	0.012	0.000	21.826	16.952	2.44	84.8	36.22	351.81	1.09
600	43.033	0.013	0.000	14.629	51.335	7.49	89.9	38.69	373.44	0.62
650	49.795	0.016	0.144	28.620	98.148	17.15	83.0	41.34	396.40	0.51
690	41.195	0.011	0.514	3.835	86.049	25.61	97.4	40.12	385.85	0.39
725	40.653	0.012	0.000	2.272	61.629	31.68	98.3	39.96	384.50	0.31
765	42.344	0.009	0.131	5.760	67.539	38.32	96.0	40.64	390.38	0.63
810	47.587	0.015	0.347	18.474	61.166	44.34	88.6	42.16	403.45	1.10
900	42.347	0.011	0.201	2.151	44.165	48.69	98.5	41.72	399.69	0.81
940	41.937	0.012	0.140	2.527	63.324	54.92	98.2	41.19	395.13	0.57
990	41.253	0.011	0.000	1.985	112.821	66.02	98.5	40.64	390.42	0.29
1040	41.091	0.009	0.000	1.738	142.098	80.00	98.7	40.56	389.65	0.28
1080	41.382	0.010	0.000	3.736	110.284	90.85	97.3	40.26	387.07	0.18
1120	41.959	0.009	0.000	4.553	78.855	98.61	96.7	40.59	389.97	0.45
1160	43.947	0.008	3.133	19.416	14.163	100	87.9	38.64	373.07	1.33

Temp (C)	$^{40}Ar/^{39}Ar$	$^{38}Ar/^{39}Ar$	$^{37}Ar/^{39}Ar$	$^{36}Ar/^{39}Ar$	^{39}Ar	$F^{39}Ar^{1}$	%40*[2]	$^{40}Ar^{*}/^{39}Ar_{K}$	Age (Ma)	±1σ
H-4 white mica			**J=.0059920**							
550	46.706	0.014	0.307	30.431	21.097	1.82	80.8	37.74	367.96	1.77
625	45.799	0.014	0.572	20.743	43.436	5.57	86.8	39.73	385.48	0.68
665	55.502	0.015	0.000	46.433	51.946	10.06	75.2	41.76	403.11	1.07
700	44.189	0.012	0.000	11.618	64.902	15.67	92.2	40.73	394.21	1.01
730	44.048	0.012	0.305	10.843	145.253	28.21	92.8	40.87	395.37	0.29
805	42.814	0.009	0.000	6.150	155.450	41.64	95.7	40.97	396.30	0.16
820	42.619	0.011	0.000	6.554	93.071	49.68	95.4	40.66	393.57	0.36
840	43.003	0.009	0.551	8.282	74.623	56.13	94.4	40.62	393.18	0.47
860	47.880	0.013	0.515	21.642	56.788	61.03	86.8	41.54	401.20	0.71
885	43.773	0.010	0.000	8.057	52.007	65.53	94.5	41.37	399.74	0.62
910	45.751	0.013	0.000	14.166	50.190	69.86	90.8	41.54	401.24	0.42
940	51.379	0.014	0.019	33.709	58.294	74.90	80.6	41.40	399.98	0.96
980	43.672	0.011	0.799	7.929	58.396	79.94	94.9	41.43	400.22	0.58
1020	42.681	0.011	0.226	6.326	62.443	85.34	95.6	40.82	394.99	0.62
1060	43.447	0.012	0.307	9.086	63.722	90.84	93.9	40.79	394.66	0.44
1100	43.029	0.010	0.889	6.825	51.282	95.27	95.6	41.12	397.59	1.31
1160	42.858	0.011	1.249	8.016	54.763	100	94.9	40.65	393.50	0.86
H-5 white mica			**J=.0060120**							
500	42.582	0.012	0.000	22.328	11.286	0.88	84.5	35.96	353.31	2.23
550	38.124	0.006	0.000	14.575	14.751	2.03	88.6	33.80	333.87	1.55
600	39.679	0.007	0.938	18.832	23.418	3.86	86.3	34.22	337.74	1.44
650	63.926	0.022	0.000	86.415	29.624	6.17	60.0	38.37	374.66	0.85
680	43.279	0.011	0.409	13.447	31.754	8.64	90.9	39.34	383.23	0.96
720	41.451	0.006	0.473	7.907	65.512	13.75	94.5	39.16	381.64	0.52
780	40.570	0.007	0.172	2.043	133.618	24.17	98.5	39.97	388.72	0.35
795	41.614	0.009	0.474	5.877	137.319	34.88	95.9	39.93	388.34	0.43
810	41.964	0.009	0.486	5.562	98.888	42.59	96.2	40.37	392.22	0.48
825	41.767	0.008	0.436	5.743	82.716	49.04	96.0	40.11	389.97	0.62
840	43.094	0.010	0.205	10.797	73.261	54.75	92.6	39.91	388.21	0.60
860	47.715	0.015	0.737	24.377	53.043	58.89	85.1	40.60	394.22	1.41
880	42.488	0.010	0.786	12.023	50.986	62.87	91.9	39.03	380.47	0.64
910	42.266	0.008	0.000	10.221	49.406	66.72	92.8	39.22	382.18	0.42
940	42.887	0.012	0.675	12.109	52.027	70.78	91.8	39.39	383.60	0.41
980	41.764	0.011	0.000	9.161	57.633	75.27	93.5	39.04	380.53	0.61
1030	41.903	0.011	0.000	10.030	75.671	81.17	92.9	38.92	379.49	0.47
1080	42.399	0.011	0.558	6.716	79.211	87.35	95.5	40.47	393.14	0.71
1130	41.638	0.010	0.048	5.398	105.406	95.57	96.1	40.03	389.23	0.51
1180	43.128	0.011	1.043	11.702	56.829	100	92.3	39.80	387.25	0.57
H-6B white mica			**J=.0060068**							
500	46.997	0.004	0.048	28.297	5.548	2.08	82.2	38.62	376.58	2.53
550	44.227	0.002	0.056	19.573	7.204	4.79	86.9	38.43	374.90	1.48
600	44.428	0.002	0.024	26.769	13.187	9.74	82.2	36.50	357.81	0.80
650	74.446	0.002	0.010	111.623	20.184	17.32	55.7	41.44	401.24	1.17
700	42.400	0.001	0.002	7.901	72.019	44.36	94.4	40.04	389.07	0.45
760	41.842	0.001	0.011	4.974	25.532	53.95	96.4	40.35	391.76	0.48
775	41.685	0.002	0.004	4.251	15.994	59.95	96.9	40.41	392.24	0.59
800	43.486	0.002	0.005	8.565	13.193	64.91	94.1	40.93	396.83	0.83
825	44.280	0.001	0.004	12.074	15.654	70.79	91.9	40.69	394.71	0.74
860	61.338	0.001	0.014	66.637	13.851	75.99	67.9	41.63	402.85	2.52
895	45.887	0.003	0.025	16.597	13.316	80.99	89.3	40.96	397.09	0.70
930	41.486	0.000	0.024	10.558	13.923	86.21	92.4	38.35	374.18	0.97
980	43.189	0.000	0.015	9.762	16.595	92.45	93.3	40.28	391.17	1.10
1030	43.352	0.000	0.014	7.405	20.120	100	94.9	41.14	398.66	1.28

Temp (C)	$^{40}Ar/^{39}Ar$	$^{38}Ar/^{39}Ar$	$^{37}Ar/^{39}Ar$	$^{36}Ar/^{39}Ar$	^{39}Ar	$F^{39}Ar$[1]	%40*[2]	$^{40}Ar^*/^{39}Ar_K$	Age (Ma)	±1σ
	H-7 biotite		**J=.0059860**							
500	58.143	0.001	0.119	116.494	4.275	0.36	40.8	23.71	239.58	4.15
550	43.752	0.000	0.024	46.226	5.040	0.78	68.7	30.07	298.79	3.30
600	46.119	0.002	0.000	29.232	13.992	1.96	81.2	37.46	365.18	1.41
650	54.400	0.002	0.003	49.591	52.409	6.36	73.0	39.72	385.07	0.73
690	40.801	0.001	0.002	3.684	84.413	13.44	97.3	39.69	384.77	1.03
710	40.941	0.001	0.000	2.819	62.787	18.71	97.9	40.09	388.22	0.69
730	40.784	0.000	0.000	2.819	60.299	23.77	97.9	39.93	386.85	0.45
750	40.303	0.000	0.000	3.186	45.201	27.56	97.6	39.34	381.71	0.36
775	45.634	0.001	0.000	19.920	38.354	30.78	87.1	39.73	385.08	0.65
800	43.964	0.002	0.007	14.714	31.467	33.42	90.1	39.60	383.94	0.84
835	43.577	0.000	0.001	11.669	33.850	36.27	92.0	40.11	388.41	0.70
870	41.125	0.001	0.007	4.128	34.158	39.13	97.0	39.88	386.46	0.69
910	41.513	0.001	0.006	5.231	36.515	42.20	96.2	39.95	387.00	0.48
950	41.147	0.001	0.005	3.294	82.278	49.10	97.6	40.15	388.80	0.23
1000	40.825	0.001	0.004	1.762	292.850	73.68	98.7	40.28	389.94	0.38
1050	40.284	0.003	0.001	1.419	198.765	90.37	98.9	39.84	386.10	0.34
1085	40.360	0.001	0.005	1.669	91.682	98.06	98.7	39.85	386.13	0.47
1120	41.186	0.001	0.000	2.814	23.100	100	97.9	40.33	390.37	0.30
	H-8 biotite		**J=.0059780**							
500	97.331	0.046	6.088	207.239	13.226	0.88	38.0	36.95	360.22	3.89
550	60.623	0.020	0.235	68.345	21.084	2.29	66.7	40.44	390.83	1.08
600	48.511	0.013	0.101	25.936	86.058	8.05	84.2	40.84	394.30	0.38
640	46.838	0.014	0.168	19.253	221.833	22.88	87.9	41.15	397.00	0.47
670	42.911	0.010	0.095	6.142	275.473	41.29	95.8	41.09	396.45	0.21
690	42.301	0.012	0.105	3.788	200.631	54.70	97.3	41.18	397.22	0.18
710	42.630	0.010	0.000	3.634	114.471	62.36	97.4	41.53	400.31	0.35
730	42.625	0.010	0.105	5.626	47.106	65.50	96.1	40.96	395.32	0.74
760	43.789	0.013	1.316	7.037	23.591	67.08	95.7	41.88	403.34	1.17
800	43.044	0.011	1.462	5.820	46.738	70.21	96.5	41.52	400.20	0.60
850	50.173	0.015	0.000	25.312	51.517	73.65	85.0	42.67	410.12	0.85
900	42.843	0.011	0.988	3.405	52.856	77.18	97.9	41.96	404.01	0.59
950	42.779	0.011	0.114	5.460	108.976	84.47	96.2	41.16	397.08	0.37
1000	42.655	0.010	0.167	4.767	119.561	92.46	96.7	41.25	397.85	0.44
1050	42.155	0.010	0.552	4.650	69.892	97.13	96.9	40.84	394.31	0.51
1100	42.712	0.010	2.581	5.240	34.733	99.46	97.2	41.53	400.25	0.54
1150	49.420	0.020	7.487	30.668	8.152	100	83.9	41.45	399.60	2.46

1) Cumulative ^{39}Ar gas released during the experiment (%).
2) %40 = % radiogenic ^{40}Ar of total ^{40}Ar released.*